

## Journal Pre-proofs

Luminescent complexes of iridium(III) with aliphatic amines and detection of biogenic amines

Victor García-Calvo, José García-Calvo, Iván Fernández-Espinosa, Arancha Carbayo, María José Rojo, M<sup>a</sup> Teresa Rodríguez, Gabriel García-Herbosa, Tomás Torroba, José Vicente Cuevas

PII: S0020-1693(19)31398-2  
DOI: <https://doi.org/10.1016/j.ica.2019.119409>  
Reference: ICA 119409

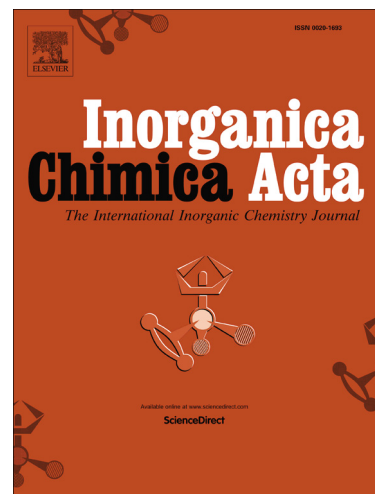
To appear in: *Inorganica Chimica Acta*

Received Date: 10 September 2019  
Revised Date: 22 November 2019  
Accepted Date: 30 December 2019

Please cite this article as: V. García-Calvo, J. García-Calvo, I. Fernández-Espinosa, A. Carbayo, M. José Rojo, M.T. Rodríguez, G. García-Herbosa, T. Torroba, J. Vicente Cuevas, Luminescent complexes of iridium(III) with aliphatic amines and detection of biogenic amines, *Inorganica Chimica Acta* (2019), doi: <https://doi.org/10.1016/j.ica.2019.119409>

This is a PDF file of an article that has undergone enhancements after acceptance, such as the addition of a cover page and metadata, and formatting for readability, but it is not yet the definitive version of record. This version will undergo additional copyediting, typesetting and review before it is published in its final form, but we are providing this version to give early visibility of the article. Please note that, during the production process, errors may be discovered which could affect the content, and all legal disclaimers that apply to the journal pertain.

© 2019 Published by Elsevier B.V.



## Luminescent complexes of iridium(III) with aliphatic amines and detection of biogenic amines

Victor García-Calvo, José García-Calvo, Iván Fernández-Espinosa, Arancha Carbayo, María José Rojo, M<sup>a</sup> Teresa Rodríguez, Gabriel García-Herbosa, Tomás Torroba, José Vicente Cuevas<sup>jvcv@ubu.es</sup>

Departamento de Química, Facultad de Ciencias, Universidad de Burgos, Plaza de Misael Bañuelos s/n, 09001 Burgos, Spain

**Abstract**

The straightforward reaction of  $[\text{Ir}_2(\text{ppy})_4(\mu\text{-Cl})_2]$  with an excess of aliphatic amines yields luminescent iridium complexes of general formula  $[\text{IrCl}(\text{ppy})_2(\text{amine})]$  [amine = *n*-octylamine (**1**), *t*-butylamine (**2**), piperidine (**3**)]. The higher sterical hindrance of the amine in complex **2** was the responsible of its equilibrium with the starting materials. The luminescence of **1** and **3** has been studied showing emission at 508 and 509 nm respectively. As the aliphatic amines can be considered models of biogenic amines, this luminescence has been used to explore the viability of this reaction in the detection of biogenic amines. The exposition to vapors of biogenic amines of a solution of  $[\text{Ir}_2(\text{ppy})_4(\mu\text{-Cl})_2]$  in  $\text{CH}_2\text{Cl}_2$  or in different solid supports, showed that it was possible to detect the amines in a quick and easy way, with limits of detection value (in solution of methylene chloride) of 4.8  $\mu\text{M}$  for cadaverine.

**1. Introduction**

Over the last years, luminescent iridium complexes have received great interest due to their possibilities in fields such as optoelectronics,<sup>[1-3]</sup> bioimaging<sup>[4,5]</sup> and chemosensors.<sup>[1,2,6-9]</sup> The luminescent properties of these iridium complexes are due to their high quantum efficiency and color tunability. The highly efficient emission of these complexes is attributed to strong spin-orbit coupling of the metal leading to singlet-triplet mixing due to the heavy atom effect. Most of the complexes studied in these contexts have the structure of two cyclometalating ( $\text{N}^{\wedge}\text{C}$ ) ligands and a third chelating ( $\text{N}^{\wedge}\text{N}$ ), ( $\text{N}^{\wedge}\text{C}$ ), ( $\text{N}^{\wedge}\text{O}$ ) or ( $\text{O}^{\wedge}\text{O}$ ) ligand coordinated to iridium(III). Iridium(III) complexes with two cyclometalating ( $\text{N}^{\wedge}\text{C}$ ) ligands and two monodentate ligands have been studied as well.<sup>[10]</sup> Nevertheless, neutral complexes with two cyclometalating ( $\text{N}^{\wedge}\text{C}$ ) ligands and one non-chelating nitrogen donor ligand along with a halogen ligand completing the coordination are less abundant.<sup>[10-16]</sup> Among these complexes, only two examples display amines coordinated to the iridium.<sup>[11,15]</sup> Coordination of amines to iridium compounds can generate luminescent compounds offering a way to detect these kinds of amines. A group of amines of interest to be detected are the biogenic amines which constitute a potential public health concern due to their physiological and toxicological effects. The consumption of foods containing high concentrations of biogenic amines has been associated with health hazards.<sup>[17]</sup> In the literature there are described several detection protocols of biogenic amines.<sup>[18]</sup> The quantitative determination of biogenic amines is generally accomplished by chromatographic methods,<sup>[19,20]</sup> although the use of these methods are limited by extended analysis times as well as expensive and large instrumentation. Alternatively to chromatography, other techniques such as the use of sensors,<sup>[21]</sup> colorimetric assays<sup>[22,23]</sup>

or flow injection analysis<sup>[24]</sup> have been proposed as analytical methods to biogenic amines.

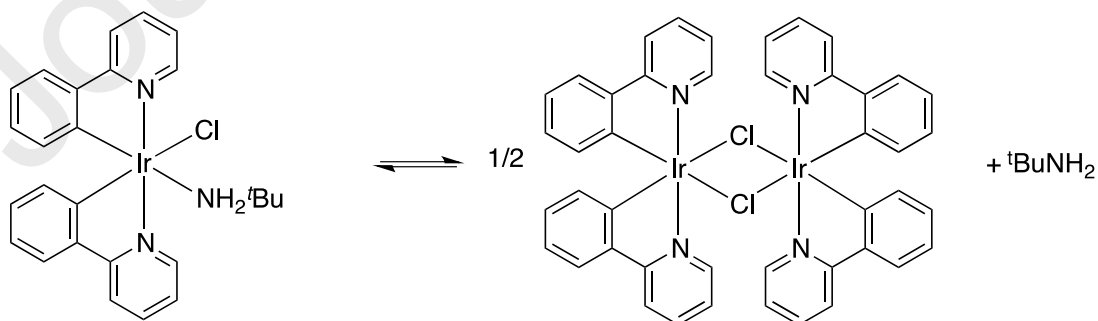
In this work we present the coordination of simple primary aliphatic amines to iridium yielding luminescent iridium complexes. The formation of these luminescent complexes is applied to the detection of biogenic amines.

## 2. Results and discussion

Reaction of the chloride-bridged dimer  $[\text{Ir}_2(\text{ppy})_4(\mu\text{-Cl})_2]$  (ppy = deprotonated phenylpyridine) with an excess of aliphatic amines yielded the corresponding neutral complexes with *n*-octylamine, *t*-butylamine and piperidine (see scheme 1). Additionally, no reaction was observed in the same conditions using triethylamine as nitrogen donor base. The products of these reactions have been characterized by <sup>1</sup>H NMR, FT/IR spectroscopy, and mass analysis (see experimental section). In the case of compound **1**, single crystals suitable for X-ray diffraction were obtained.

The <sup>1</sup>H NMR spectra of these complexes show a set of signals belonging to the aromatic protons of the two nonequivalent orthometallated phenylpyridine ligands, along with the signals belonging to amine ligands.

It is not observed the formation of the cationic complexes in which two amine ligands coordinate to the iridium (displacing the chlorido ligands). Sterical hindrance is important in the solution behavior of these complexes. Compounds **1** and **3** (with ligands *n*-octylamine and piperidine respectively) show clean signals in the NMR spectrum (see Figure S2 and Figure S3), while compound **2** (with *t*-butylamine) the <sup>1</sup>H NMR spectrum in deuterated chloroform (see Figure S1) shows a mixture of signals belonging to the iridium complex with the amine coordinate and signals belonging to the chloride-bridged dimer  $[\text{Ir}_2(\text{ppy})_4(\mu\text{-Cl})_2]$  as well as free amine. The addition of an excess of amine to this solution removed the signals of the dimer leaving the signals of the iridium complex with the coordinated amine and signals of free amine in excess, indicating the presence of an equilibrium in solution (see Scheme 2 and Figure S1 in Supporting Information).



**Scheme 2**

As said above, no reaction was observed with a more hindered amine such as triethylamine.

### Solid-state characterization of **1**.

Single crystals of **1** were grown by slow evaporation of chloroform solutions of this complex. Compound **1** crystallizes in the trigonal group R-3. The structure of this complex shows the Ir atom in a distorted octahedral geometry. The metal center is coordinated by two N atoms and two C atoms from two phenylpyridinate ligands, as well as one N atom from an *n*-octylamine ligand and one Cl atom. As can be seen in the ORTEP plot in Figure 1 the formation of complex **1** is completely regioselective, i.e. only C,C-cis-N,N-trans isomer is obtained (as it occurs in other complexes of iridium with chelating C-N ligands). The crystal is build up by weak interactions between  $\Delta$ - $\Delta$  enantiomers, while interactions  $\Delta$ - $\Delta$  or  $\Lambda$ - $\Lambda$  hydrogen bonding are not formed (Figure 2 and Figures S11 and S12).

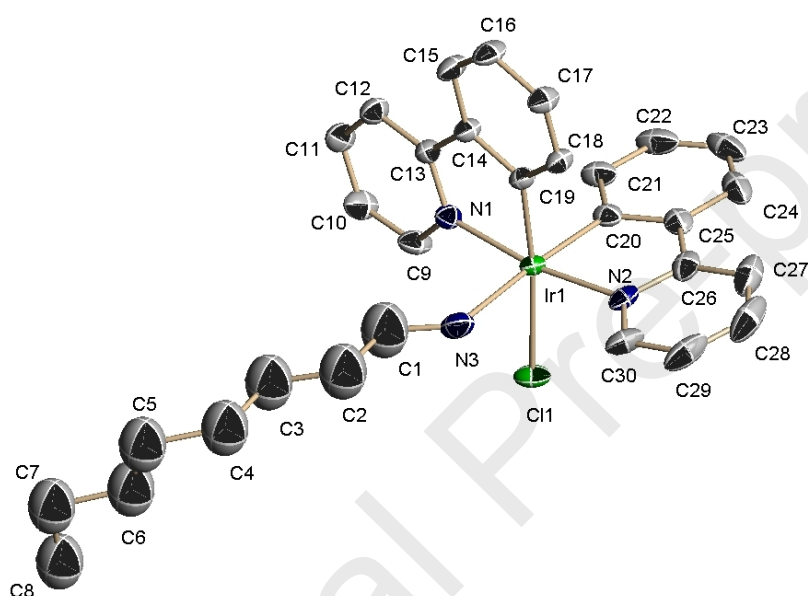


**Figure 1.** Structure of the  $\Lambda$ -1. Hydrogen atoms omitted for clarity and ellipsoids plotted at 50% probability level. Selected bond parameters: Ir1-C19 = 1.991(4), Ir1-C20 = 2.001(4), Ir1-N2 = 2.043(4), Ir1-N1 = 2.048(4), Ir1-N3 = 2.197(4), Ir1-Cl1 = 2.4654(4) Å; C20-Ir1-N2 = 80.11(17)°, C19-Ir1-N1 = 80.63(16)°, N2-Ir1-N1 = 170.89(15)°, C20-Ir1-N3 = 175.68(18)°, C19-Ir1-Cl1 = 173.85(12)°, N3-Ir1-Cl1 = 83.88(12)°.

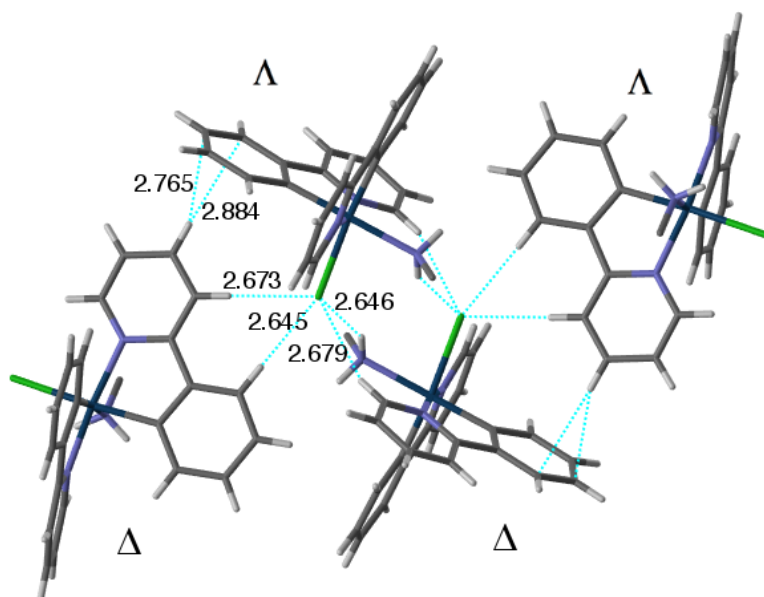


**Figure 2.** Intermolecular bonding showing interactions between  $\Delta$ - $\Lambda$  enantiomers. The values of the distances refer to weak interactions between the chlorido ligand of a  $\Lambda$ -enantiomer and hydrogen atoms of two different  $\Delta$ -enantiomers. Weak contacts between C-H bond and a neighbor ring are shown as well. Octyl chain has been shortened for clarity.

### Photophysical Study.

The absorption and emission spectra of complexes **1** and **3** were recorded in degassed dichloromethane at room temperature (see Figure 3). These complexes displayed very similar absorption spectra with strong bands at about 260 nm (values of extinction coefficients in experimental section), moderate bands at ca. 300-400 nm, and less intense tailing bands beyond 400 nm, which was attributed to spin-allowed  $^1\text{IL}$  ( $\pi \rightarrow \pi^*$ ) ( $\text{N}^{\wedge}\text{C}$ ),  $^1\text{MLCT}$  ( $d(\text{Ir}) \rightarrow \pi^*(\text{N}^{\wedge}\text{C})$ ), and spin-forbidden  $^3\text{MLCT}$  ( $d(\text{Ir}) \rightarrow \pi^*(\text{N}^{\wedge}\text{C})$ ) transitions, respectively as found in related compounds.<sup>[11,12,25]</sup> These complexes exhibited intense greenish emission (under excitation wavelength of 397 nm) in methylene chloride at room temperature. Strong, broad and nonstructured emissions were found. These emissions displayed maxima 508 nm, 535 nm (sh) for **1** and 509 nm, 535 nm (sh) for **3**. It is interesting to notice the coincidence of the values for complexes **1** and **3**, indicating the analogy of orbitals involved in the electronic transitions independently of the nature (primary or secondary) of the amine coordinated to the iridium center. The photoluminescence quantum yield (PLQY) displayed essentially the same value for both complexes (10.0 and 10.5% for **1** and **3** respectively) in good agreement with the strong similarity of their electronic structure (see Figure 5 and Figure S7). To the best of our knowledge, no PLQY of analogous examples to our compounds have been reported. In order to compare the PLQY of our compounds we think that complexes with two cyclometalating ( $\text{N}^{\wedge}\text{C}$ ) ligands and a third chelating amino acid ligand ( $\text{N}^{\wedge}\text{O}$ ) coordinated to iridium(III) could be an interesting option, as our complexes have two cyclometalating ( $\text{N}^{\wedge}\text{C}$ ) ligands, a N-donor ligand and a chlorido ligand. The values reported here are close to the reported values for complexes with proline ( $\text{N}^{\wedge}\text{O}$  ligand) that have values of 3.5 and 2.3 (in methylene chloride) with

ppy as (N<sup>^</sup>C) ligand<sup>[26]</sup> or **18** and **7.6** (in methanol) with deprotonated 2-phenylquinoline as (N<sup>^</sup>C) ligand.<sup>[27]</sup>

**Table 1.** Photophysical Properties in CH<sub>2</sub>Cl<sub>2</sub> solution of **1** and **3**.

Complex	$\lambda_{em}^{max}$ [nm] <sup>a</sup>	$\tau$ [ns] <sup>b</sup>	PLQY [%] <sup>c</sup>
<b>1</b>	508	158	10.0±2
<b>3</b>	509	144	10.5±2

<sup>a</sup> $\lambda_{exc}$  = 400 nm. <sup>b</sup>Measured under an atmosphere of argon. <sup>c</sup>Excitation range 386 to 411 nm.

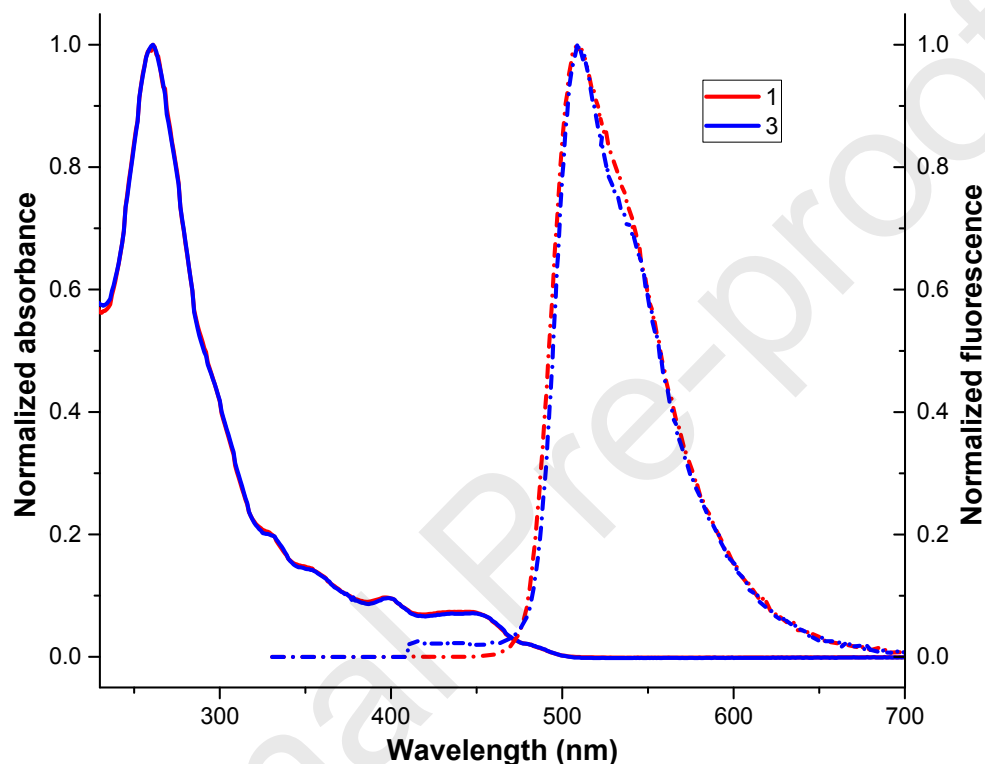


**Figure 3.** Normalized absorption (solid lines) and emission (dotted lines) spectra of **1** (red) and **3** (blue) [ $1 \cdot 10^{-5}$  M in CH<sub>2</sub>Cl<sub>2</sub> at room temperature].

### Electrochemistry

Table 2 gathers the observed potential values referenced to the redox pair ferrocenium/ferrocene following the IUPAC recommendations.<sup>[28]</sup>

**Table 2.** Electrochemical data obtained by cyclic voltammetry in this study and referenced to the redox system ferrocenium/ferrocene.<sup>a</sup>

Complex	Observed $E_{pk}^{ox}$ and $E_{pk}^{red}$ values. <sup>b</sup>		$i_{cat}(Ar)$ <sup>c</sup>
	Anodic scan	Cathodic scan	
[IrCl(ppy) <sub>2</sub> (piperidine)] ( <b>3</b> )	0.58 <sup>r,sh</sup>	-2.44, -2.69, -2.98	-39
[IrCl(ppy) <sub>2</sub> ( <i>n</i> -octylamine)] ( <b>1</b> )	0.46 <sup>r</sup> , 0.58 <sup>r</sup>	-2.46, -2.71	-42
[Ir( $\mu$ -Cl)(ppy) <sub>2</sub> ] <sub>2</sub>	0.58 <sup>r</sup> , 1.28	-2.47, -2.71,	-55

<sup>a</sup> The reduction potential mean value observed for Ferrocenium/Ferrocene (Fc<sup>+</sup>/Fc) used as internal calibrant under the employed experimental conditions was  $E^0 = 0.443 \pm 0.005$  V vs. the AgCl/Ag (saturated KCl) electrode.

<sup>b</sup> Anodic or cathodic scan peaks observed under Ar unless stated otherwise.

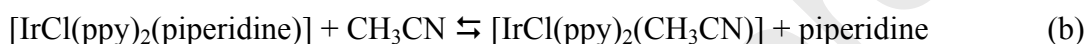
<sup>c</sup> Maximum registered cathodic current ( $\mu$ A) under Ar,  $i_{\text{cat}}(\text{Ar})$ .

<sup>r</sup> Waves where both peaks  $i_{\text{ox}}$  and  $i_{\text{red}}$  were observed. Value of  $E_{1/2}$  is given in those cases.

<sup>sh</sup> Shoulder, not resolved peaks (see Figure 4 and Figure S5 in Supporting Information).

In octahedral Ir(III) related complexes it is generally accepted that oxidations are metal-centered Ir(III)/Ir(IV) processes while reductions have been assigned both to ligand-centered and Ir(III)/Ir(I) metal-centered.<sup>[11,29-31]</sup>

In complex **3**, an apparently reversible wave is observed at  $E_{1/2} = +0.58$  V (vs ferrocenium/ferrocene) in the anodic scan. Broadening of the wave may be due to the equilibrium (b).



In the cathodic scan to negative potentials a first irreversible reduction appears at  $E_{\text{pk}}^{\text{red}} = -2.44$  V followed by also irreversible peaks at -2.69 V and -2.98 V.

A similar behavior is found for complex **1**, nevertheless, at oxidation scan a first reversible wave is revealed at +0.46 V (see Figure S5 in Supporting Information) not solved in the piperidine complex. To explain the small differences between both complexes at oxidation scans, we suggest that the one-electron oxidation of  $[\text{IrCl}(\text{ppy})_2(\text{amine})]$  to  $[\text{IrCl}(\text{ppy})_2(\text{amine})]^+$ , facilitates substitution of the amine ligand by the coordinating acetonitrile solvent to give  $[\text{IrCl}(\text{ppy})_2(\text{CH}_3\text{CN})]^+$ . Cyclic Voltammetry of the precursor dimer  $[\text{Ir}_2(\text{ppy})_4(\mu\text{-Cl})_2]$  in acetonitrile is shown in Figure S6 of the Supporting Information. A clean reversible wave is observed at +0.58 V and an irreversible peak at +1.28 V (vs Fc<sup>+</sup>/Fc) that must be due to oxidations of solvent or supporting electrolyte. The value at +0.58 V is exactly the same value observed for the complexes  $[\text{IrCl}(\text{ppy})_2(\text{amine})]$  (amine = piperidine or *n*-octylamine), and can be assigned to the  $E_{1/2}$  value for the redox pair  $[\text{IrCl}(\text{ppy})_2(\text{CH}_3\text{CN})]^+ / [\text{IrCl}(\text{ppy})_2(\text{CH}_3\text{CN})]$ . The  $E_{1/2}$  value observed for  $[\text{IrCl}(\text{ppy})_2(\textit{n}-octylamine)]<sup>+</sup> /  $[\text{IrCl}(\text{ppy})_2(\textit{n}-octylamine)]$  is +0.46 V and the  $E_{1/2}$  value for  $[\text{IrCl}(\text{ppy})_2(\text{piperidine})]^+ / [\text{IrCl}(\text{ppy})_2(\text{piperidine})]$  must be even closer to +0.58 V avoiding the observation of the wave but broadening the wave at +0.58 V. In addition, the calculated energies of the HOMO for both complexes show that this molecular orbital in complex **3** has a slightly more negative energy than the HOMO in complex **1** (-5.06 vs -5.04 eV respectively, see Figure 5 and Figure S7), in good agreement with a greater easiness for oxidation of complex **1** than for complex **3**. In summary, the observed first oxidation potential of the amine complexes  $[\text{IrCl}(\text{ppy})_2(\text{amine})]$  follows the order  $E_{1/2} [\text{IrCl}(\text{ppy})_2(\textit{n}-octylamine)] <  $E_{1/2} [\text{IrCl}(\text{ppy})_2(\text{piperidine})]$  and this fits well with the calculated energy values for the HOMO's of both complexes (see theoretical calculations).$$

The cathodic scan of the precursor dimer  $[\text{Ir}_2(\text{ppy})_4(\mu\text{-Cl})_2]$  parallels that shown by the complexes  $[\text{IrCl}(\text{ppy})_2(\text{amine})]$  (amine = piperidine or *n*-octylamine) indicating that the

LUMO is ligand (phenylpyridine) based in all cases, in good agreement with quantum chemical calculations (see below).

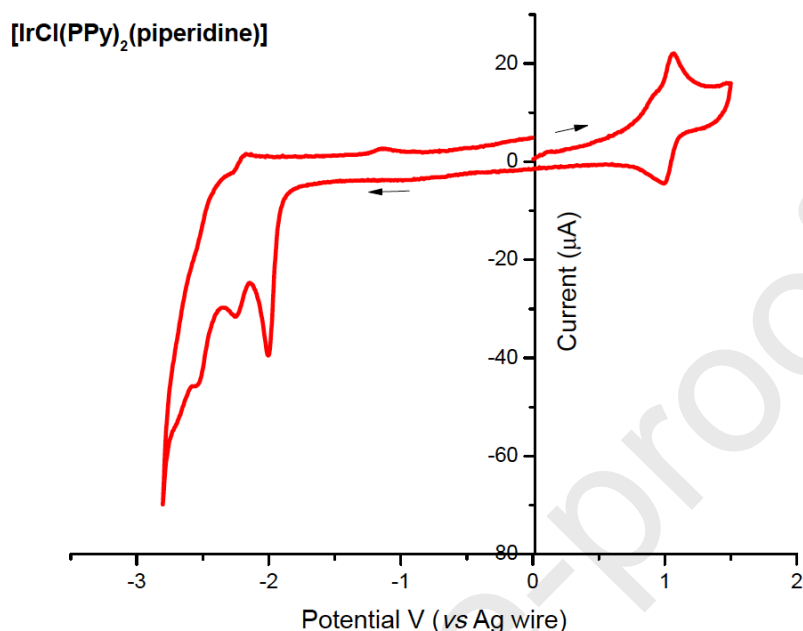


**Figure 4.** Cyclic voltammograms (0→ 1.5→ -2.8→ 0 V) of  $10^{-3}$ M  $[\text{IrCl}(\text{ppy})_2(\text{piperidine})]$  (**3**). See and Experimental Section for details.

#### Theoretical Calculations.

To gain insight into the electronic and optical properties of these compounds, DFT calculations were performed at the B3LYP/(6-31G\* + LANL2DZ) level on the  $[\text{Ir}(\text{ppy})_2(\text{L})(\text{Cl})]$  [L = *n*-octylamine (**1**) and piperidine (**3**)] complexes in dichloromethane solution.

The minimum-energy geometries calculated for the complexes **1** and **3** in their electronic ground state ( $S_0$ ) reproduce the near-octahedral coordination of the Ir metal and are in good agreement with the X-ray diffraction data presented above for **1**. For complexes **1** and **3** the calculated angle Cl-Ir- $N_{\text{amine}}$  is 85.1 and 91.7° respectively, and the angle  $N_{\text{amine}}$ -Ir- $N_{\text{amine}}$  in **1** is 87.3°.

Figure 5 displays the atomic orbital composition calculated for the HOMO and LUMO of complex **1** (complex **3** shows the same shape and energy order of this molecular orbitals, see Figure S7 in Supporting Information). It has been already reported that for related bis-heteroleptic cyclometalated with bipyridine ancillary ligands,<sup>[32–36]</sup> the HOMO is composed of a mixture of Ir(III)  $d_{\pi}$  orbitals ( $t_{2g}$ ) and  $\pi$  orbitals of the phenyl ring of the cyclometalating ligands. Although in the neutral complex **1** there is not a bipyridine related ancillary ligand, but a nitrogen donor and a chlorido ligands, the HOMO has a similar shape to the one described for cationic bipyridine derivatives and furthermore there is as well a significant participation of a Cl  $p_{\pi}$  orbital.<sup>[11,25]</sup> In addition, in those compounds where the ancillary ligand is a bipyridine derivative, the

LUMO corresponds to the  $\pi^*$  LUMO of the bipyridine fragment. But it is worth mentioning here that the amine ligand does not have any noticeable contribution in the frontier molecular orbitals in the complexes presented in this work. The ancillary ligands of the complexes described here are not aromatic and the LUMO is predominantly localized on the cyclometalating ligands.<sup>[11,25]</sup> The calculated HOMO-LUMO energy gap is 3.67 eV (3.65 eV for complex **3**).

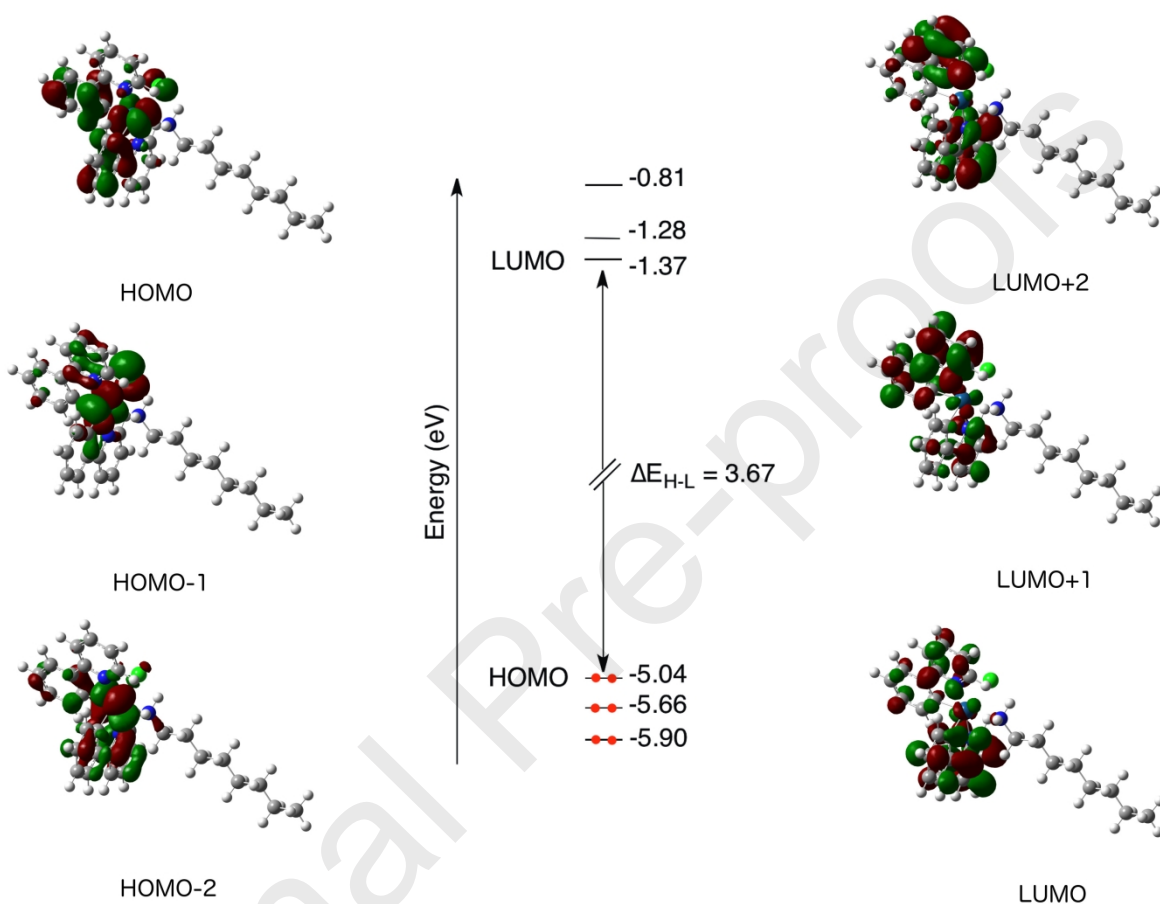


**Figure 5.** Schematic representation showing the calculated energies (eV) of the frontier and their molecular orbitals (0.3 e·au<sup>-3</sup>) for compound **1**.

The low-lying triplet states at the optimized geometries of the ground state ( $S_0$ ) of compounds **1** and **3** were calculated to investigate the nature of the emitting excited state. These calculations were developed using the time-dependent DFT (TD-DFT) approach. Table 3 summarizes the vertical excitation energies calculated for the first four triplets and two singlets, as well as their molecular orbital descriptions and electronic nature. As expected, complexes **1** and **3** present a very similar pattern. The lowest-lying triplet state ( $T_1$ ) and the next one ( $T_2$ ) are separated only by 0.05-0.08 eV. In both complexes  $T_1$  is basically described by the HOMO  $\rightarrow$  LUMO excitation and  $T_2$  the HOMO  $\rightarrow$  LUMO+1. These two transitions have a <sup>3</sup>MLCT/<sup>3</sup>LC/<sup>3</sup>LLCT nature in which the <sup>3</sup>LLCT character is due to excitations from the chlorido ligand to the cyclometalating phenylpyridinate. The third state ( $T_3$ ) implies orbitals of the iridium atom, the chlorido and the cyclometalating ligands, and it is calculated more than 0.4 eV above  $T_1$ . In both complexes the lowest-lying singlet state is described by the HOMO  $\rightarrow$  LUMO transition.

**Table 3.** Lowest Excited States Calculated at the TD-DFT B3LYP/(6-31G\* + LANL2DZ) Level for Complexes **1** and **3** in Dichlorometane Solution<sup>a</sup>

state	E (eV)	monoexcitations	nature	description	Osc. Str.
<b>1</b>					
T <sub>1</sub>	2.601	H → L (92)	$d_{\pi}(\text{Ir}) + \pi_{\text{ppy}} + p_{\pi}(\text{Cl}) \rightarrow \pi_{\text{ppy}}^*$	<sup>3</sup> MLCT/ <sup>3</sup> LC/ <sup>3</sup> LLCT	
T <sub>2</sub>	2.680	H → L+1 (81)	$d_{\pi}(\text{Ir}) + \pi_{\text{ppy}} + p_{\pi}(\text{Cl}) \rightarrow \pi_{\text{ppy}}^*$	<sup>3</sup> MLCT/ <sup>3</sup> LC/ <sup>3</sup> LLCT	
S <sub>1</sub>	2.860	H → L (100)	$d_{\pi}(\text{Ir}) + \pi_{\text{ppy}} + p_{\pi}(\text{Cl}) \rightarrow \pi_{\text{ppy}}^*$	<sup>1</sup> MLCT/ <sup>1</sup> LC/ <sup>1</sup> LLCT	0,045
S <sub>2</sub>	2.993	H → L+1 (100)	$d_{\pi}(\text{Ir}) + \pi_{\text{ppy}} + p_{\pi}(\text{Cl}) \rightarrow \pi_{\text{ppy}}^*$	<sup>1</sup> MLCT/ <sup>1</sup> LC/ <sup>1</sup> LLCT	0,07
T <sub>3</sub>	3.052	H-1 → L (22) H-1 → L+1 (31) H → L+1 (21)	$d_{\pi}(\text{Ir}) + p_{\pi}(\text{Cl}) \rightarrow \pi_{\text{ppy}}^*$ $d_{\pi}(\text{Ir}) + p_{\pi}(\text{Cl}) \rightarrow \pi_{\text{ppy}}^*$ $d_{\pi}(\text{Ir}) + \pi_{\text{ppy}} + p_{\pi}(\text{Cl}) \rightarrow \pi_{\text{ppy}}^*$	<sup>3</sup> LLCT/ <sup>3</sup> MLCT <sup>3</sup> LLCT/ <sup>3</sup> MLCT <sup>3</sup> LLCT/ <sup>3</sup> MLCT	
T <sub>4</sub>	3.103	H-2 → L (35) H → L (16)	$d_{\pi}(\text{Ir}) + \pi_{\text{ppy}} \rightarrow \pi_{\text{ppy}}^*$ $d_{\pi}(\text{Ir}) + \pi_{\text{ppy}} + p_{\pi}(\text{Cl}) \rightarrow \pi_{\text{ppy}}^*$	<sup>3</sup> MLCT/ <sup>3</sup> LC/ <sup>3</sup> LLCT <sup>3</sup> MLCT/ <sup>3</sup> LC/ <sup>3</sup> LLCT	
<b>3</b>					
T <sub>1</sub>	2.619	H → L (92)	$d_{\pi}(\text{Ir}) + \pi_{\text{ppy}} + p_{\pi}(\text{Cl}) \rightarrow \pi_{\text{ppy}}^*$	<sup>3</sup> MLCT/ <sup>3</sup> LC/ <sup>3</sup> LLCT	
T <sub>2</sub>	2.696	H → L+1 (81)	$d_{\pi}(\text{Ir}) + \pi_{\text{ppy}} + p_{\pi}(\text{Cl}) \rightarrow \pi_{\text{ppy}}^*$	<sup>3</sup> MLCT/ <sup>3</sup> LC/ <sup>3</sup> LLCT	
S <sub>1</sub>	2.879	H → L (100)	$d_{\pi}(\text{Ir}) + \pi_{\text{ppy}} + p_{\pi}(\text{Cl}) \rightarrow \pi_{\text{ppy}}^*$	<sup>1</sup> MLCT/ <sup>1</sup> LC/ <sup>1</sup> LLCT	0,043
S <sub>2</sub>	3.006	H → L+1 (100)	$d_{\pi}(\text{Ir}) + \pi_{\text{ppy}} + p_{\pi}(\text{Cl}) \rightarrow \pi_{\text{ppy}}^*$	<sup>1</sup> MLCT/ <sup>1</sup> LC/ <sup>1</sup> LLCT	0,005
T <sub>3</sub>	3.066	H-1 → L (22) H-1 → L+1 (31) H → L+1 (23)	$d_{\pi}(\text{Ir}) + p_{\pi}(\text{Cl}) \rightarrow \pi_{\text{ppy}}^*$ $d_{\pi}(\text{Ir}) + p_{\pi}(\text{Cl}) \rightarrow \pi_{\text{ppy}}^*$ $d_{\pi}(\text{Ir}) + \pi_{\text{ppy}} + p_{\pi}(\text{Cl}) \rightarrow \pi_{\text{ppy}}^*$	<sup>3</sup> LLCT/ <sup>3</sup> MLCT <sup>3</sup> LLCT/ <sup>3</sup> MLCT <sup>3</sup> MLCT/ <sup>3</sup> LC/ <sup>3</sup> LLCT	
T <sub>4</sub>	3.090	H-2 → L (37) H → L (16)	$d_{\pi}(\text{Ir}) + \pi_{\text{ppy}} \rightarrow \pi_{\text{ppy}}^*$ $d_{\pi}(\text{Ir}) + \pi_{\text{ppy}} + p_{\pi}(\text{Cl}) \rightarrow \pi_{\text{ppy}}^*$	<sup>3</sup> MLCT/ <sup>3</sup> LC/ <sup>3</sup> LLCT <sup>3</sup> MLCT/ <sup>3</sup> LC/ <sup>3</sup> LLCT	

<sup>a</sup>Vertical excitation energies (E), dominant monoexcitations with contributions (within parenthesis) of >15% the nature of the electronic transition and the description of the excited state are summarized.

The geometry of the lowest-lying triplet state was optimized using the UB3LYP (spin-unrestricted) approach to further confirm the nature of the emitting triplet. Table 4 summarizes the values of the adiabatic energy difference between S<sub>0</sub> and T<sub>1</sub> ( $\Delta E$ ) as well as the emission energy ( $E_{\text{em}}$ ) that has been estimated as the vertical energy difference between T<sub>1</sub> and S<sub>0</sub> at the optimized minimum-energy geometry of T<sub>1</sub>. The order of the estimated emission energies matches with the experimental order.

**Table 4.** The adiabatic energy difference between S<sub>0</sub> and T<sub>1</sub> ( $\Delta E$ ) and the emission energy ( $E_{\text{em}}$ ) estimated as the vertical energy difference between T<sub>1</sub> and S<sub>0</sub> at the optimized minimum-energy geometry of T<sub>1</sub>.

Complex	$\Delta E$ (eV)	$E_{\text{em}}$ (eV; nm)
1	2.39	2.29; 542.1
3	2.41	2.27; 546.9

The Figure 6 (and Table S6) shows the unpaired-electron spin-density distributions found for the lowest-energy triplet state. The complexes **1** and **3** show analogous spin density spreading the ppy-Ir environment with little contribution of the chlorido ligand and the nitrogen atom of the amine ligand (Ir ~ 0.45e, C<sup>N</sup> ligands ~ 1.50e) that matches the topology of the HOMO → LUMO excitation indicating electron transfer from the iridium center to the orthometalated ppy, intraligand ppy and ppy to ppy. This supports the <sup>3</sup>LLCT/<sup>3</sup>MLCT/<sup>3</sup>LC nature predicted for the emitting state by the TD-DFT

calculations and it is in good agreement with the shape broad and unstructured of the bands observed in the photoluminescence.

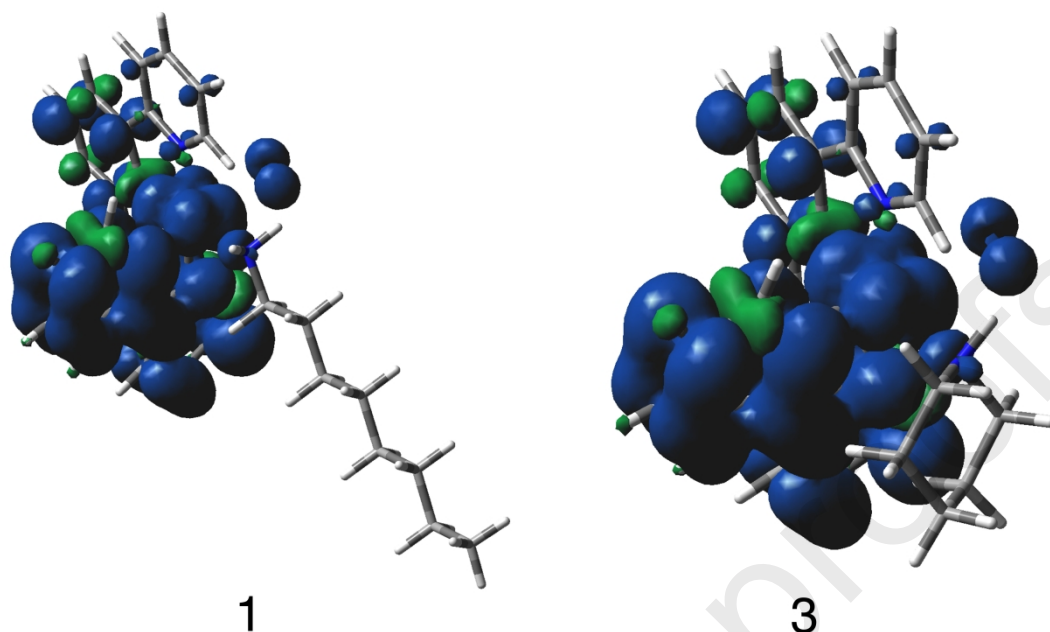


**Figure 6.** Unpaired-electron spin-density contours (0.006 au) calculated for the  $T_1$  triplet states of compounds **1** and **3**.

#### Detection of biogenic amines.

The straightforward formation of these compounds prompted us to explore the possibility to test this reaction in the detection of aliphatic amines increasing/changing luminescence. The amines used in the formation of the complexes described above could be considered simplified models of amines that exist in nature such as the biogenic amines that can be found as the product of degradation of food<sup>[17]</sup>. In this study the biogenic amines we deeply studied as representative examples were cadaverine (pentane-1,5-diamine) and phenylethylamine.

The effect over luminescence was studied by performing titrations with these two biogenic amines. Figure 7 shows the titration in luminescence of a solution in methylene chloride of the complex of iridium  $[\text{Ir}_2(\text{ppy})_4(\mu\text{-Cl})_2]$  in the presence of increasing quantities of cadaverine.

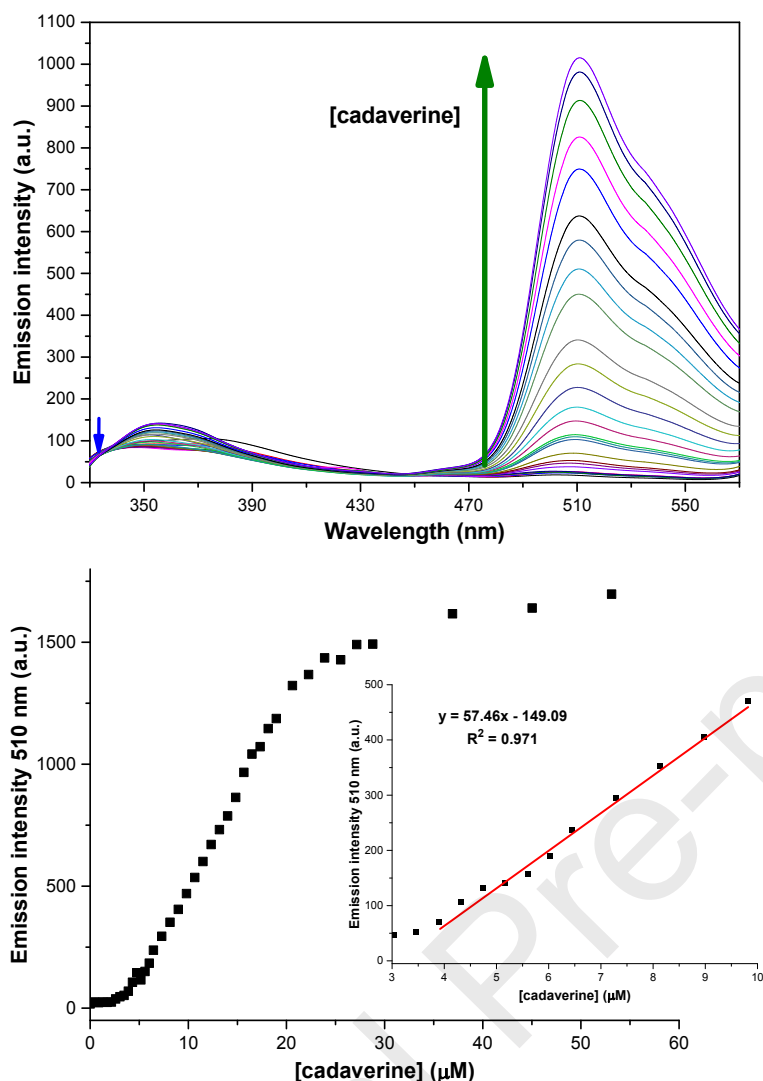


**Figure 7.** Titration in fluorescence of  $[\text{Ir}_2(\text{ppy})_4(\mu\text{-Cl})_2]$   $10 \mu\text{M}$  in DCM in presence of increasing quantities of cadaverine.  $\lambda_{\text{exc}} = 300 \text{ nm}$ .

It may be seen how the fluorescence in green (510 nm band) increased with the amine concentration. In fact, the compound presented a sigmoidal response in which the fluorescence increase was calculated to be noticeable at a concentration around  $4.8 \mu\text{M}$  (limit of detection, calculated with the linear regression, when the probability of false positive ( $\alpha$ ) and false negative ( $\beta$ ) is equal or inferior to 5 %. Performed with the program “R” v.2.7).

As shown in Figure 8, similar results were obtained for the detection of phenylethylamine, the fluorescence in blue from the initial complex  $[\text{Ir}_2(\text{ppy})_4(\mu\text{-Cl})_2]$  decreased and the luminescence in green, 510 nm, increased. Nevertheless the calculated value for the limit of detection (using the same method) is  $34.0 \mu\text{M}$ , which is higher than the one found for the cadaverine. These values are comparable to other published colorimetric methods for histidine that report values of  $\sim 5 \mu\text{M}$ <sup>[23]</sup> and concentrations between 0.1 and 1.0 mM.<sup>[22]</sup>

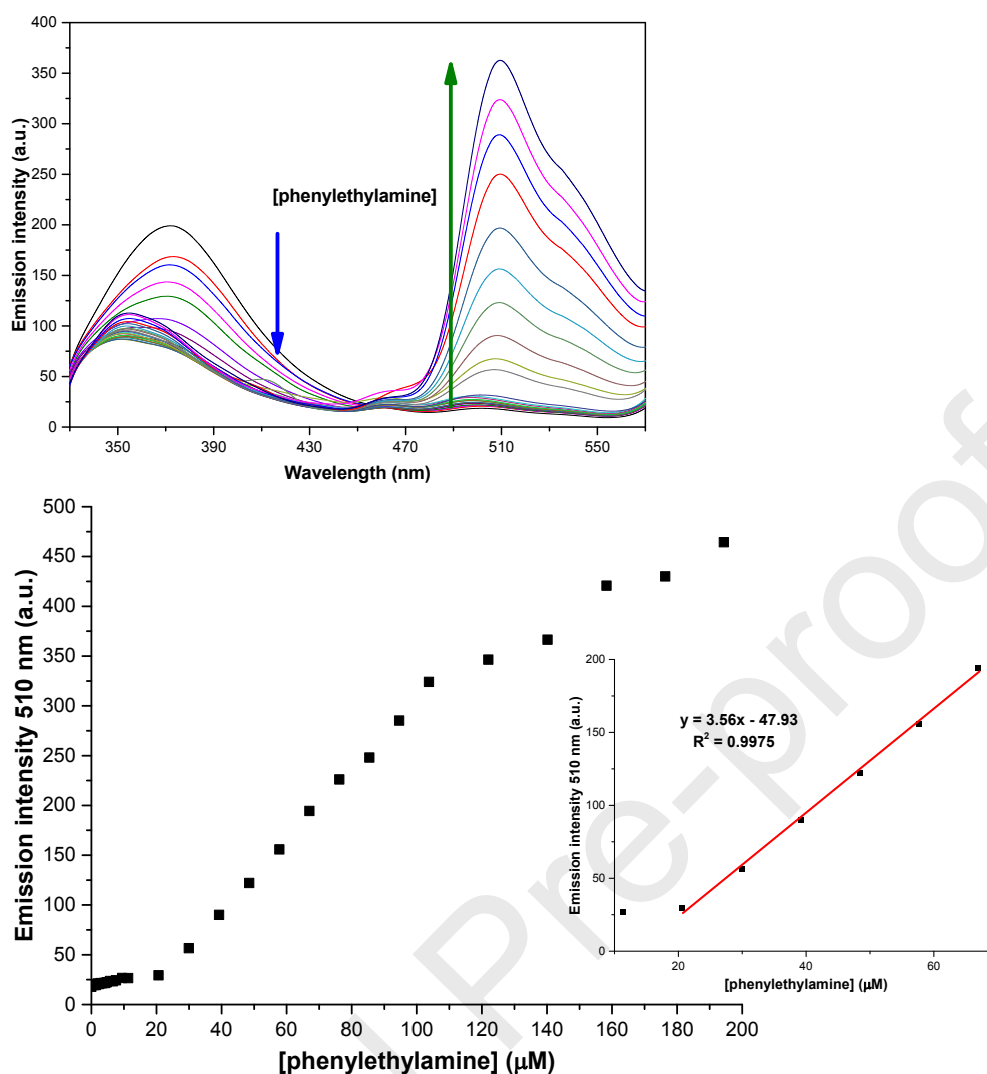


**Figure 8.** Titration in fluorescence of  $[\text{Ir}_2(\text{ppy})_4(\mu\text{-Cl})_2]$   $10 \mu\text{M}$  in DCM and in presence of increasing quantities of phenylethylamine.  $\lambda_{\text{exc}} = 300 \text{ nm}$ .

To test the viability of this reaction to the detection of amines, solutions of  $[\text{Ir}_2(\text{ppy})_4(\mu\text{-Cl})_2]$  in methylene chloride were exposed to vapors of different amines. The Figure 9 shows the different response of the tested amines. As a result, it was observed that the amines that produced vapors at room temperature (i.e. the more volatile amines) increased the final luminescence. The observed order was Putrescine > Cadaverine > Spermidine > Phenylethylamine; and no significant change for the rest of the amines from the test.

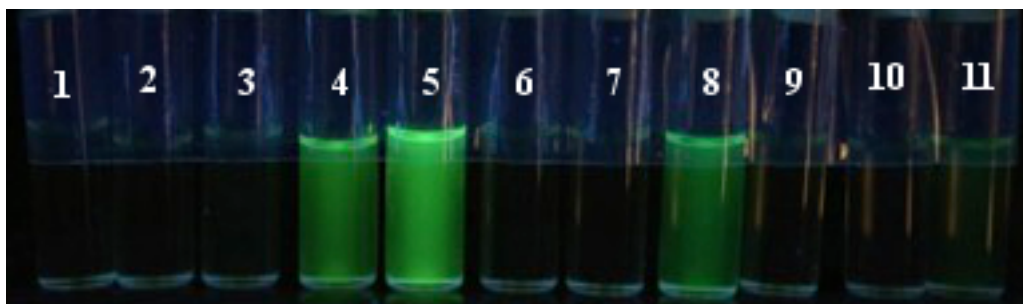


**Figure 9.** Behavior of  $[\text{Ir}_2(\text{ppy})_4(\mu\text{-Cl})_2]$  ( $10 \mu\text{M}$  in  $\text{CH}_2\text{Cl}_2$ ) in presence of vapors of different amines. From left to right reference (1), probe + air (2), probe +  $\text{N}_2$  (3), probe + cadaverine (4), probe + putrescine (5), probe + spermine (6), probe + tyramine (7), probe + spermidine (8), probe + histamine (9), probe + tryptamine (10), probe + phenylethylamina (11).

Solids are handled better than solutions. For this reason, the possibility to support the complex of iridium,  $[\text{Ir}_2(\text{ppy})_4(\mu\text{-Cl})_2]$ , on solid materials was explored as well. Small pieces of filter paper and TLC plates (see Experimental Section) were embedded in  $10 \mu\text{M}$  solutions of  $[\text{Ir}_2(\text{ppy})_4(\mu\text{-Cl})_2]$  and the ensemble complex-support was exposed to amine vapors over a period of 24 hours. Both, the filter paper and the chromatography plates with the iridium complex gave signal under UV light ( $366 \text{ nm}$ ) after its exposure to vapors of putrescine (see Figure 10).

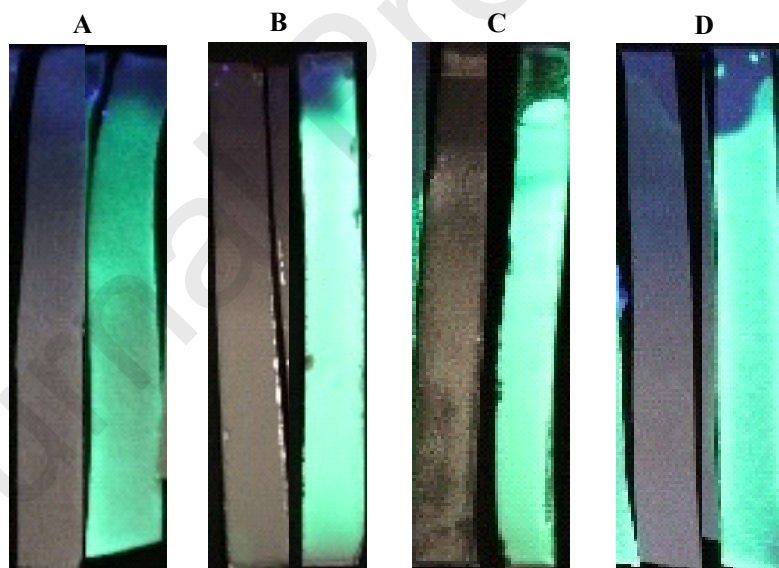


**Figure 10.** Embedded samples under  $366 \text{ nm}$  light, before (left) and after (right) being in contact with putrescine vapors (24h). A) Filter paper, B) TLC plate, C) Filter paper A + polyvinyl alcohol (PVA), D) Filter paper B. (See Experimental Section to know the characteristics of the Filter papers and the chromatography plate).

The iridium complex supported on filter paper or chromatography plates was able to produce signal under UV light ( $366 \text{ nm}$ ) after exposure to vapor of volatile amines (Figure 11).

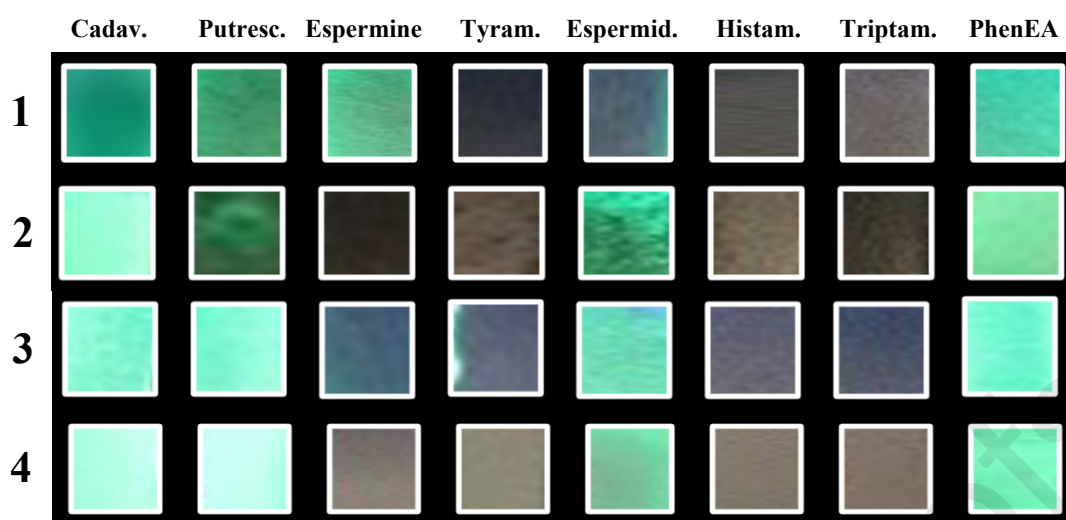


**Figure 11.** Embedded filter paper type A (row 1), filter paper type A + PVA (row 2), filter paper type B (row 3) and TLC plates (row 4) samples under 366 nm light, after being in contact with vapors of different amines (24h).

The experiments with the iridium complex supported on filter paper or chromatography plates indicate that it is possible to easily detect vapors of the different volatile amines as it was performed in methylene chloride solution of the complex. All supports used are able to produce signal when the system is exposed to vapors of volatile biogenic amines and the intensity order was very similar in both systems solution and supported, Putrescine > Cadaverine > Espermidine = Phenylethylamine.

## Conclusions

Aliphatic amines such as *n*-octylamine, *t*-butylamine and piperidine react easily with  $[\text{Ir}_2(\text{ppy})_4(\mu\text{-Cl})_2]$  at room temperature yielding products with high luminescence. This reaction is partially conditioned by the sterical nature of the reacting amine. The products of these reactions have been fully characterized displaying an interesting electrochemistry and luminescence emitting green light. The excited state was theoretically calculated displaying a topology of HOMO  $\rightarrow$  LUMO excitation. This luminescence has been tested to detect biogenic amines. The exposition to vapors of biogenic amines of a solution of  $[\text{Ir}_2(\text{ppy})_4(\mu\text{-Cl})_2]$  in methylene chloride afforded a limit of detection of 4.8  $\mu\text{M}$  for cadaverine. When the same iridium compound on different solid supports was exposed to vapors of amines it was possible to detect vapors of the different volatile amines in a quick and easy way, and the intensity order was very similar in all cases (different supports), Putrescine > Cadaverine > Espermidine = Phenylethylamine. This method can offer some advantages such as simple handling and simple instrumentation.

## EXPERIMENTAL SECTION

**General.** Solvents were dried prior to use and stored under nitrogen. 2-phenylpyridine, *n*-octylamine, *t*-butylamine, piperidine, biogenic amines and  $\text{IrCl}_3 \cdot x\text{H}_2\text{O}$  were commercial grade and were used without further purification. The dimeric starting material  $[\text{Ir}(\mu\text{-Cl})(\text{ppy})_2]_2$  was synthesized according to published methods.<sup>[37]</sup> The solid supports for the complex  $[\text{Ir}(\mu\text{-Cl})(\text{ppy})_2]_2$  used in the detection of biogenic amines tests were (A) filter paper medium flow rate 185 mm QLPG-185-100B), (B) filter paper MF support Pads, AP10 37 mm. AP10037X, and TLC Silica gel 60 aluminium sheets (Merck) 1.16835.0001. The supports were cut into strips of a size of 5mm x 50mm. Then, these strips were plunged in a 10  $\mu\text{M}$  solution of  $[\text{Ir}(\mu\text{-Cl})(\text{ppy})_2]_2$  in chloroform until they are completely wet. The strips were removed from the solution and dried in air, leaving the iridium complex supported in the strips.

**Characterization.** Elemental analyses (C, H, N) were performed with a LECO CHNS-932 apparatus. Infrared spectra were recorded with a Jasco FT/IR-4200 spectrophotometer (4000-400  $\text{cm}^{-1}$  range), as KBr disks.  $^1\text{H}$  and  $^{13}\text{C}$  NMR spectra were obtained on a VARIAN UNITY INOVA spectrometer operating at 400 and 100 MHz, respectively, and using  $\text{SiMe}_4$  as internal standard at 20  $^\circ\text{C}$ , and a VARIAN MERCURY 300 MHz spectrometer using  $\text{SiMe}_4$  as internal standard at 20  $^\circ\text{C}$ . ESI-HRMS Mass spectra (position of the peaks in Da) were recorded with an Agilent 6545 Q-TOF equipment. The experimentally obtained  $m/z$  values are expressed in Da and the isotopic distribution matches that of calculated minutes.

**Measurements of UV/Vis absorption and luminescence spectra:** UV/Vis absorption spectra were recorded on a Hitachi U-3900 spectrophotometer, whereas excitation, emission spectra and excited state lifetimes were recorded on a FLS980 spectrofluorometer from Edinburgh Instruments. Samples were prepared under argon atmosphere using Schlenk techniques. The luminescence emission spectra were first recorded by exciting at the maximum absorption wavelength of the corresponding UV/Vis absorption spectra. Once the maximum emission wavelength is determined in this experiment, an excitation scan for this emission was carried out to determine the maximum excitation wavelength, which was used later on to obtain the optimized emission spectra. Luminescence quantum yields were measured by coupling the system with an integration sphere from Edinburgh instruments with an absolute error of  $\pm 2\%$  (information of the manufacturer of the equipment).

**Electrochemistry:** Electrochemical measurements were carried out with PalmSens 3 potentiostats (available range -5V to +5V, software PStace4 Version 4.4.2). Unless otherwise stated CV's were scanned at 200  $\text{mVs}^{-1}$ , in acetonitrile (5 ml), 0.1M  $n\text{-Bu}_4\text{PF}_6$  supporting electrolyte, purging with Ar at room temperature through a PTFE tubing. Working electrodes were of glassy carbon (3 mm diameter). The auxiliary electrode was a platinum wire. The reference electrodes used were Ag/AgCl (saturated KCl) MF-2052 BASi separated from the bulk solution by a "thirsty" Vycor<sup>TM</sup> frit or a silver wire pseudo-reference electrode. Ferrocene was added at the end of the experiments. The observed ferrocenium/ferrocene couple was  $E_{1/2} = 0.443 \pm 0.005 \text{ V vs. Ag/AgCl}$ . Potential values measured with the Ag wire are plenty of uncertainty and, at the end of the experiment, measures were carried out with the Ag/AgCl (saturated KCl) electrode.

**Theoretical calculations:** Density functional theory (DFT) calculations were carried out with the D.01 revision of the Gaussian 09 package,<sup>[38]</sup> using the Becke's three-parameter B3LYP exchange-correlation functional,<sup>[39,40]</sup> together with the 6-31G(d) basis set for H, C, N, O, F, and S,<sup>[41,42]</sup> and the "double-z" quality LANL2DZ basis set for the Ir element.<sup>[43]</sup> The geometries of the singlet ground state ( $S_0$ ) and the lowest-energy triplet state ( $T_1$ ) were fully optimized without imposing any symmetry restriction. The geometries of the triplet states were calculated at the spin-unrestricted UB3LYP level with a spin multiplicity of 3. All the calculations were performed in the presence of the solvent (dichloromethane). Solvent effects were considered within the self-consistent reaction field (SCRF) theory using the SMD keyword that performs a polarized continuum model (PCM)<sup>[44]</sup> calculation using the solvation model of Thrular et al.<sup>[45]</sup> Time-dependent DFT (TD-DFT) calculations of the lowest-lying 20 singlets and triplets were performed in the presence of the solvent at the minimum-energy geometry optimized for the ground state ( $S_0$ ).

**X-ray crystallography:** A summary of crystal data collection and refinement parameters for **1** are given in Table S7 in Supporting Information. A single crystal of **1** was coated in high-vacuum grease, mounted on a glass fiber. X-ray measurements were made using a Bruker D8 VENTURE PhotonIII area-detector diffractometer with Mo- $K_\alpha$  radiation ( $\lambda = 0.71073 \text{ \AA}$ ).<sup>[46]</sup> The diffraction pattern was indexed and the unit cell was refined using SAINT.<sup>[47]</sup> Absorption corrections were applied, based on multiple and symmetry-equivalent measurements.<sup>[48]</sup> The structure was solved by ShelXT structure solution program using Intrinsic Phasing and refined with the XL refinement package using Least Squares minimisation.<sup>[49]</sup> All non-hydrogen atoms were assigned anisotropic displacement parameters and refined without positional constraints. All other hydrogen atoms were constrained to ideal geometries and refined with fixed isotropic displacement parameters.

**[Ir(ppy)<sub>2</sub>(C<sub>8</sub>H<sub>19</sub>N)(Cl)] (1).** In a 100 ml round-bottom flask were added 100 mg (0.093 mmol) of [Ir<sub>2</sub>(ppy)<sub>4</sub>( $\mu$ -Cl)<sub>2</sub>] and then 10 ml of chloroform. To the yellow slurry were slowly added 73 mg (0.565 mmol) of *n*-octylamine. The mixture was stirred for 30 minutes. During the stirring a clean yellow solution was formed that was filtered through celite. After partial elimination of the solvent by vacuum evaporation and addition of hexane a yellow precipitate was collected (111,2 mg, yield 90%). Anal.Calc. (found) for C<sub>30</sub>H<sub>35</sub>N<sub>3</sub>ClIr·0.2CHCl<sub>3</sub>: C, 52.66 (53.16); H, 5.15 (5.30); N, 6.10 (6.32)%. <sup>1</sup>H NMR (400 MHz, Chloroform-*d*)  $\delta$ =9.86 (d,  $J = 5.8$  Hz, 1H), 8.42 (d,  $J = 5.6$  Hz, 1H), 7.90 (m, 1H), 7.84 (m, 1H), 7.76 (m, 2H), 7.52 (d,  $J = 7.7$  Hz, 2H), 7.23 (m, 2H), 6.82 (td,  $J = 7.5, 1.3$  Hz, 1H), 6.77 (td,  $J = 7.5, 1.3$  Hz, 1H), 6.69 (tdd,  $J = 7.3, 4.6, 1.4$  Hz, 2H), 6.28 (d,  $J = 7.6$  Hz, 1H), 6.15 (d,  $J = 7.6$ , 1H), 2.90 (td,  $J = 11.0, 4.6$  Hz, 1H), 2.75 (td,  $J = 11.0, 4.6$  Hz, 1H), 2.11 (m, 2H), 1.22 (m, 4H), 1.15 (m, 3H), 1.02 (m, 3H), 0.86 (t,  $J = 7.2$  Hz, 3H) ppm. FTIR (KBr pellet): 3296, 3231  $\nu$ (N-H); 3043, 2920, 2851  $\nu$ (C-H); 1606, 1582, 1478  $\delta$ (C-N and C-C aromatic) cm<sup>-1</sup>. ESI-HRMS Calculated ([M-Cl]<sup>+</sup>)  $m/z$  630.2460, found ([M-Cl]<sup>+</sup>)  $m/z$  630.2471 (Figure S7). UV-Vis absorbance maximum (CHCl<sub>3</sub>): 261 nm ( $\epsilon = 31194$ ).

**[Ir(ppy)<sub>2</sub>(C<sub>4</sub>H<sub>11</sub>N)(Cl)] (2).** In a 100 ml round-bottom flask were added 50 mg (0.047 mmol) of [Ir<sub>2</sub>(ppy)<sub>4</sub>( $\mu$ -Cl)<sub>2</sub>] and then 10 ml of chloroform. To the yellow slurry were slowly added 10 mg (0.137 mmol) of *t*-butylamine. The mixture was stirred for 30

minutes. During the stirring a clean yellow solution was formed that was filtered through celite. After partial elimination of the solvent by vacuum evaporation and addition of hexane a yellow precipitate was collected (55.9 mg, yield 98%). Anal.Calc. (found) for  $C_{26}H_{27}N_3ClIr \cdot 0.33CHCl_3$ : C, 48.74 (49.36); H, 4.25 (4.28); N, 6.47 (5.96)%.  $^1H$  NMR (400 MHz, Chloroform-*d*, excess of *t*-butylamine)  $\delta$ =9.76 (d,  $J$  = 5.8 Hz, 1H), 8.64 (d,  $J$  = 5.8 Hz, 1H), 7.78 (d,  $J$  = 8.2 Hz, 1H), 7.75 (d,  $J$  = 10.6 Hz, 1H), 7.67 (m, 2H), 7.41 (m, 1H), 7.37 (d,  $J$  = 7.6 Hz, 1H), 7.14 (dt,  $J$  = 13.9, 6.4 Hz, 2H), 6.69 (t,  $J$  = 7.4 Hz, 1H), 6.64 (t,  $J$  = 7.3 Hz, 1H), 6.60 – 6.50 (m, 2H), 6.28 (d,  $J$  = 7.6 Hz, 1H), 5.84 (d,  $J$  = 7.5 Hz, 1H), 0.80 (s, 9H) ppm. FTIR (KBr pellet): 3289, 3244  $\nu$ (N–H); 3064, 3033, 2954  $\nu$ (C–H); 1606, 1582, 1476  $\delta$ (C–N and C–C aromatic)  $cm^{-1}$ . ESI-HRMS Calculated ( $[M-Cl]^+$ )  $m/z$  574.1834, found ( $[M-Cl]^+$ )  $m/z$  574.1829 (Figure S8). UV-Vis absorbance maximum ( $CHCl_3$ ): 260 nm ( $\epsilon$  = 28420).

**[Ir(ppy)<sub>2</sub>(C<sub>5</sub>H<sub>11</sub>N)(Cl)] (3).** In a 100 ml round-bottom flask were added 50 mg (0.047 mmol) of  $[Ir_2(ppy)_4(\mu-Cl)_2]$  and then 10 ml of chloroform. To the yellow slurry were slowly added 11 mg (0.129 mmol) of piperidine. The mixture was stirred for 30 minutes. During the stirring a clean yellow solution was formed that was filtered through celite. After partial elimination of the solvent by vacuum evaporation and addition of hexane a yellow precipitate was collected (56,5 mg, yield 97%). Anal.Calc. (found) for  $C_{27}H_{27}N_3ClIr \cdot 3CHCl_3$ : C, 36.79 (37.05); H, 3.09 (3.10); N, 4.29 (4.06)%.  $^1H$  NMR (400 MHz, Chloroform-*d*)  $\delta$ =9.77 (d,  $J$  = 5.9 Hz, 1H), 8.33 (d,  $J$  = 5.9 Hz, 1H), 7.91 (d,  $J$  = 8.0 Hz, 1H), 7.84 (d,  $J$  = 8.1 Hz, 1H), 7.78 (m, 2H), 7.52 (d,  $J$  = 7.7 Hz, 2H), 7.23 (m, 2H), 6.82 (t,  $J$  = 7.5 Hz, 1H), 6.75 (t,  $J$  = 7.5 Hz, 1H), 6.67 (m, 2H), 6.20 (d,  $J$  = 7.6 Hz, 1H), 6.07 (d,  $J$  = 7.6 Hz, 1H), 3.68 (d,  $J$  = 10.6 Hz, 1H), 3.03 (d,  $J$  = 14.4 Hz, 1H), 2.86 (s br, 1H), 2.70 (s br, 1H), 1.50 (m, 6H) ppm. FTIR (KBr pellet): 3192  $\nu$ (N–H); 3057, 2930, 2847  $\nu$ (C–H); 1606, 1580, 1478  $\delta$ (C–N and C–C aromatic)  $cm^{-1}$ . ESI-HRMS Calculated ( $[M-Cl]^+$ )  $m/z$  586.1834, found ( $[M-Cl]^+$ )  $m/z$  586.1838 (Figure S9)

CCDC 1934846 contains the supplementary crystallographic data for **1**. These data are provided free of charge by The Cambridge Crystallographic Data Centre.

## CONFLICTS OF INTEREST

There are no conflicts to declare.

## ACKNOWLEDGMENT

We gratefully acknowledge financial support from the Ministerio de Economía y Competitividad, Spain (Project CTQ2015-71353-R), Junta de Castilla y León, Consejería de Educación y Cultura y Fondo Social Europeo (Project BU263P18) and Junta de Castilla y León, Consejería de Educación (Project BU087G19).

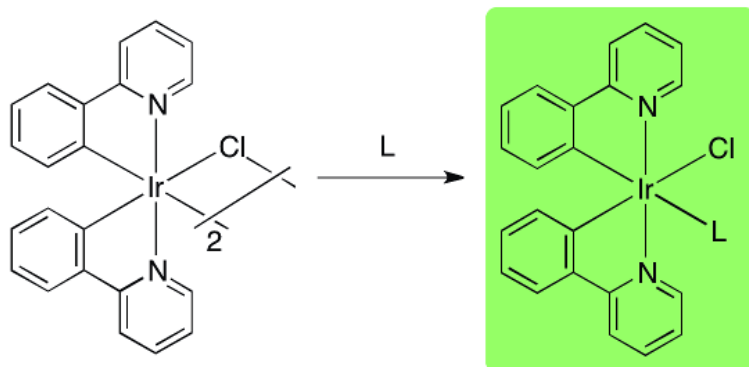
**Keywords:** Carbon dioxide reduction • Iridium • Platinum group complexes • Quantum Chemistry • Sensors

## REFERENCES

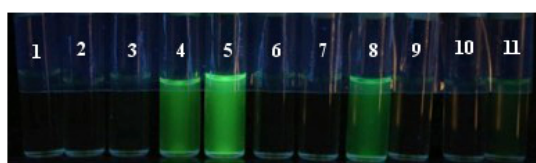
- [1] L. Flamigni, A. Barbieri, C. Sabatini, B. Ventura, F. Barigelletti, in *Photochem. Photophysics Coord. Compd. II* (Eds.: V. Balzani, S. Campagna), Springer Berlin Heidelberg, Berlin, Heidelberg, **2007**, pp. 143–203.
- [2] M. S. Lowry, S. Bernhard, *Chem. - A Eur. J.* **2006**, *12*, 7970–7977.
- [3] A. M. Bünzli, A. Pertegás, C. Momblona, J. M. Junquera-Hernández, E. C. Constable, H. J. Bolink, E. Ortí, C. E. Housecroft, *Dalton Trans.* **2016**, *45*, 16379–16392.
- [4] K. Y. Zhang, S. Liu, Q. Zhao, F. Li, W. Huang, in *Lumin. Photoactive Transit. Met. Complexes as Biomol. Probes Cell. Reagents* (Ed.: K.K.-W. Lo), Springer Berlin Heidelberg, Berlin, Heidelberg, **2015**, pp. 131–180.
- [5] Y. You, *Curr. Opin. Chem. Biol.* **2013**, *17*, 699–707.
- [6] D.-L. Ma, S. Lin, W. Wang, C. Yang, C.-H. Leung, *Chem. Sci.* **2017**, *8*, 878–889.
- [7] Q. Ma, W. Dong, Z. Ma, X. Lv, Y. Li, Q. Duan, *Mater. Lett.* **2019**, *249*, 120–123.
- [8] Q. Zhao, F. Li, C. Huang, *Chem. Soc. Rev.* **2010**, *39*, 3007–3030.
- [9] Z. Liu, Z. Bian, C. Huang, in *Mol. Organomet. Mater. Opt.* (Eds.: H. Bozec, V. Guerschais), Springer Berlin Heidelberg, Berlin, Heidelberg, **2010**, pp. 113–142.
- [10] E. Baranoff, I. Jung, R. Scopelliti, E. Solari, M. Grätzel, M. K. Nazeeruddin, *Dalt. Trans.* **2011**, *40*, 6860.
- [11] P. Alam, G. Kaur, A. Sarmah, R. K. Roy, A. R. Choudhury, I. R. Laskar, *Organometallics* **2015**, *34*, 4480–4490.
- [12] M. C. DeRosa, P. J. Mosher, G. P. A. Yap, K.-S. Focsaneanu, R. J. Crutchley, C. E. B. Evans, *Inorg. Chem.* **2003**, *42*, 4864–4872.
- [13] L. Yang, A. von Zelewsky, H. P. Nguyen, G. Muller, G. Labat, H. Stoeckli-Evans, *Inorganica Chim. Acta* **2009**, *362*, 3853–3856.
- [14] J. Li, P. I. Djurovich, B. D. Alleyne, I. Tsyba, N. N. Ho, R. Bau, M. E. Thompson, *Polyhedron* **2004**, *23*, 419–428.
- [15] R. Urban, R. Krämer, S. Mihan, K. Polborn, B. Wagner, W. Beck, *J. Organomet. Chem.* **1996**, *517*, 191–200.
- [16] C. Li, X.-Q. Dong, Q. Wang, C.-X. Ren, Y.-Q. Ding, *Acta Crystallogr. Sect. E Struct. Reports Online* **2008**, *64*, m1205–m1205.
- [17] C. Ruiz-Capillas, A. Herrero, *Foods* **2019**, *8*, 62.
- [18] M. Papageorgiou, D. Lambropoulou, C. Morrison, E. Kłodzińska, J. Namieśnik, J. Płotka-Wasyłka, *TrAC - Trends Anal. Chem.* **2018**, *98*, 128–142.
- [19] G. I. Mohammed, A. S. Bashammakh, A. A. Alsibai, H. Alwael, M. S. El-Shahawi, *TrAC Trends Anal. Chem.* **2016**, *78*, 84–94.
- [20] J. L. Ordóñez, A. M. Troncoso, M. D. C. García-Parrilla, R. M. Callejón, *Anal. Chim. Acta* **2016**, *939*, 10–25.
- [21] N. Kaur, S. Chopra, G. Singh, P. Raj, A. Bhasin, S. K. Sahoo, A. Kuwar, N. Singh, *J. Mater. Chem. B* **2018**, *6*, 4872–4902.
- [22] B. Lee, R. Scopelliti, K. Severin, *Chem. Commun.* **2011**, *47*, 9639.
- [23] P.-Q. Leng, F.-L. Zhao, B.-C. Yin, B.-C. Ye, *Chem. Commun.* **2015**, *51*, 8712–8714.
- [24] C. Ruiz-Capillas, A. M. Herrero, F. Jimenez-Colmenero, in *Flow Inject. Anal. Food Addit.* (Eds.: C. Ruiz-Capillas, L.M.L. Nollet), CRC Press, **2015**, pp. 675–690.
- [25] V. Chandrasekhar, B. Mahanti, P. Bandipalli, K. Bhanuprakash, *Inorg. Chem.* **2012**, *51*, 10536–10547.

- [26] L.-P. Li, S.-Y. Yao, Y.-L. Ou, L.-Q. Wei, B.-H. Ye, *Organometallics* **2017**, *36*, 3257–3265.
- [27] L.-P. Li, H.-L. Peng, L.-Q. Wei, B.-H. Ye, *Inorg. Chem.* **2019**, *58*, 785–793.
- [28] G. Gritzner, J. Kuta, G. Gritzner, J. Kuta, *Pure Appl. Chem.* **1984**, *56*, 461–466.
- [29] Y.-Y. Chang, J.-Y. Hung, Y. Chi, J.-P. Chyn, M.-W. Chung, C.-L. Lin, P.-T. Chou, G.-H. Lee, C.-H. Chang, W.-C. Lin, *Inorg. Chem.* **2011**, *50*, 5075–5084.
- [30] K. K.-W. Lo, J. S.-W. Chan, L.-H. Lui, C.-K. Chung, *Organometallics* **2004**, *23*, 3108–3116.
- [31] L. M. Vogler, B. Scott, K. J. Brewer, *Inorg. Chem.* **1993**, *32*, 898–903.
- [32] R. D. Costa, E. Ortí, H. J. Bolink, S. Graber, S. Schaffner, M. Neuburger, C. E. Housecroft, E. C. Constable, *Adv. Funct. Mater.* **2009**, *19*, 3456–3463.
- [33] F. De Angelis, S. Fantacci, N. Evans, C. Klein, S. M. Zakeeruddin, J.-E. Moser, K. Kalyanasundaram, H. J. Bolink, M. Grätzel, M. K. Nazeeruddin, *Inorg. Chem.* **2007**, *46*, 5989–6001.
- [34] A. B. Tamayo, S. Garon, T. Sajoto, P. I. Djurovich, I. M. Tsyba, R. Bau, M. E. Thompson, *Inorg. Chem.* **2005**, *44*, 8723–32.
- [35] C. D. Ertl, C. Momblona, A. Pertegás, J. M. Junquera-Hernández, M.-G. LaPlaca, A. Prescimone, E. Ortí, C. E. Housecroft, E. C. Constable, H. J. Bolink, *J. Am. Chem. Soc.* **2017**, *139*, 3237–3248.
- [36] D. Tordera, M. Delgado, E. Ortí, H. J. Bolink, J. Frey, M. K. Nazeeruddin, E. Baranoff, *Chem. Mater.* **2012**, *24*, 1896–1903.
- [37] S. Sprouse, K. A. King, P. J. Spellane, R. J. Watts, *J. Am. Chem. Soc.* **1984**, *106*, 6647–6653.
- [38] M. J. Frisch, G. W. Trucks, H. B. Schlegel, G. E. Scuseria, M. A. Robb, J. R. Cheeseman, G. Scalmani, V. Barone, B. Mennucci, G. A. Petersson, et al., **2013**.
- [39] A. D. Becke, *J. Chem. Phys.* **1993**, *98*, 5648–5652.
- [40] C. T. Lee, W. T. Yang, R. G. Parr, *Phys. Rev. B* **1988**, *37*, 785–789.
- [41] P. C. Hariharan, J. A. Pople, *Theor. Chim. Acta* **1973**, *28*, 213–222.
- [42] M. M. Francl, W. J. Pietro, W. J. Hehre, J. S. Binkley, M. S. Gordon, D. J. DeFrees, J. A. Pople, *J. Chem. Phys.* **1982**, *77*, 3654–3665.
- [43] P. J. Hay, W. R. Wadt, *J. Chem. Phys.* **1985**, *82*, 299–310.
- [44] G. Scalmani, M. J. Frisch, *J. Chem. Phys.* **2010**, *132*, 114110.
- [45] A. V Marenich, C. J. Cramer, D. G. Truhlar, *J. Phys. Chem. B* **2009**, *113*, 6378–6396.
- [46] Bruker. APEX3 V2016.7 Bruker AXS Inc. Bruker Instrument Service: Madison, WI, USA, **2016**.
- [47] Bruker. SAINT v8.38a. Bruker AXS Inc.: Madison, WI, USA, **2017**.
- [48] Bruker. SADABS-2016/2; Bruker AXS Inc. Madison, WI, USA. Bruker ASX Inc.: Madison, WI, USA, **2016**.
- [49] G. M. Sheldrick, *Acta Crystallogr. Sect. A* **2008**, *64*, 112–122.

Table of Contents graphical abstract.



L = aliphatic amines



L = BIOGENIC AMINES

The formation of luminescent iridium complexes with primary and secondary aliphatic amines is described. The luminescence of the complexes can be used in the detection of biogenic amines

**Keywords:** Iridium • Platinum group complexes • Quantum Chemistry • Sensors • Biogenic amines

SUPPORTING INFORMATION

PHOSPHORESCENT COMPLEXES OF IRIDIUM(III) WITH ALIPHATIC AMINES  
AND DETECTION OF BIOGENIC AMINES

Authors: Victor García Calvo, José García Calvo, Iván Fernández Espinosa, Arancha Carbayo, María José Rojo, M<sup>a</sup> Teresa Rodríguez, Gabriel García Herbosa, Tomás Torroba, José Vicente Cuevas.

Index

**1.- NMR Characterization**

Figures S1-S3

**2.- Electrochemistry**

Figures S4-S6

**3.- Quantum Chemical Calculations.**

Figure S7

Tables S1-S6

Chart S1

**4.- ESI\_HRMS**

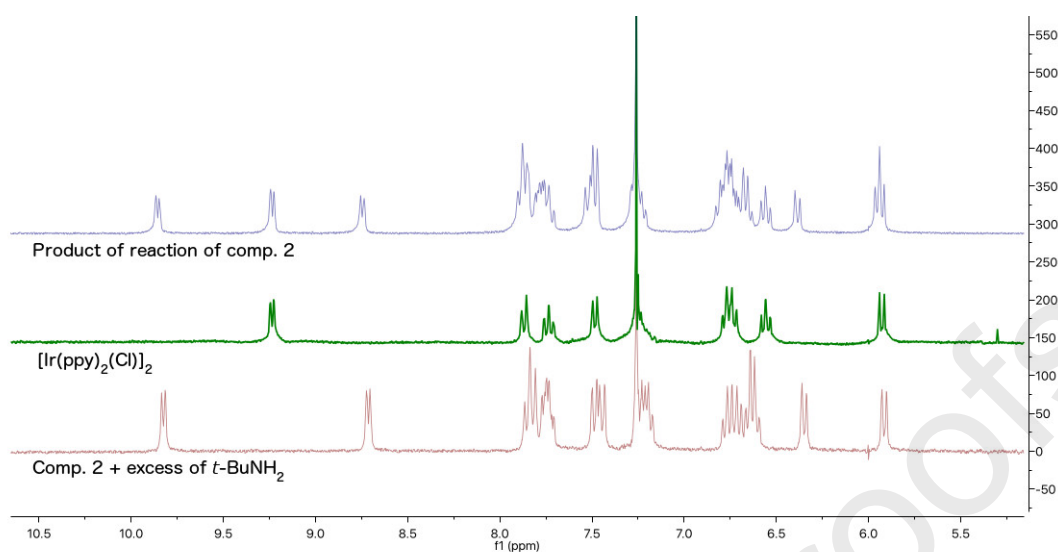
Figures S8-S10

**5.- Structural Characterization**

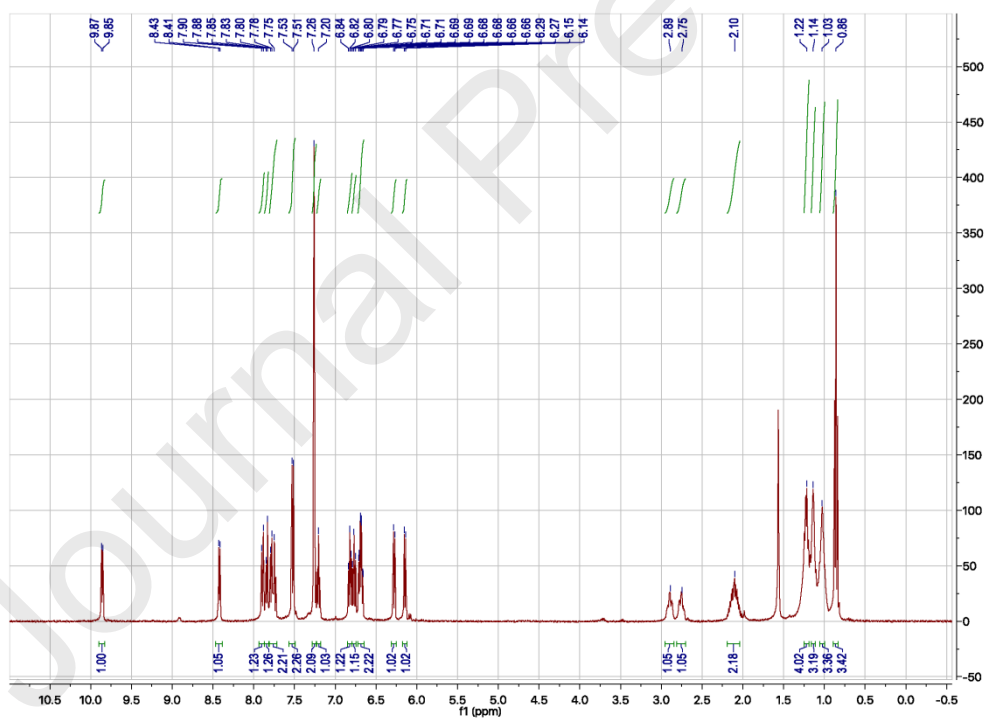
Table S7

Figure S11

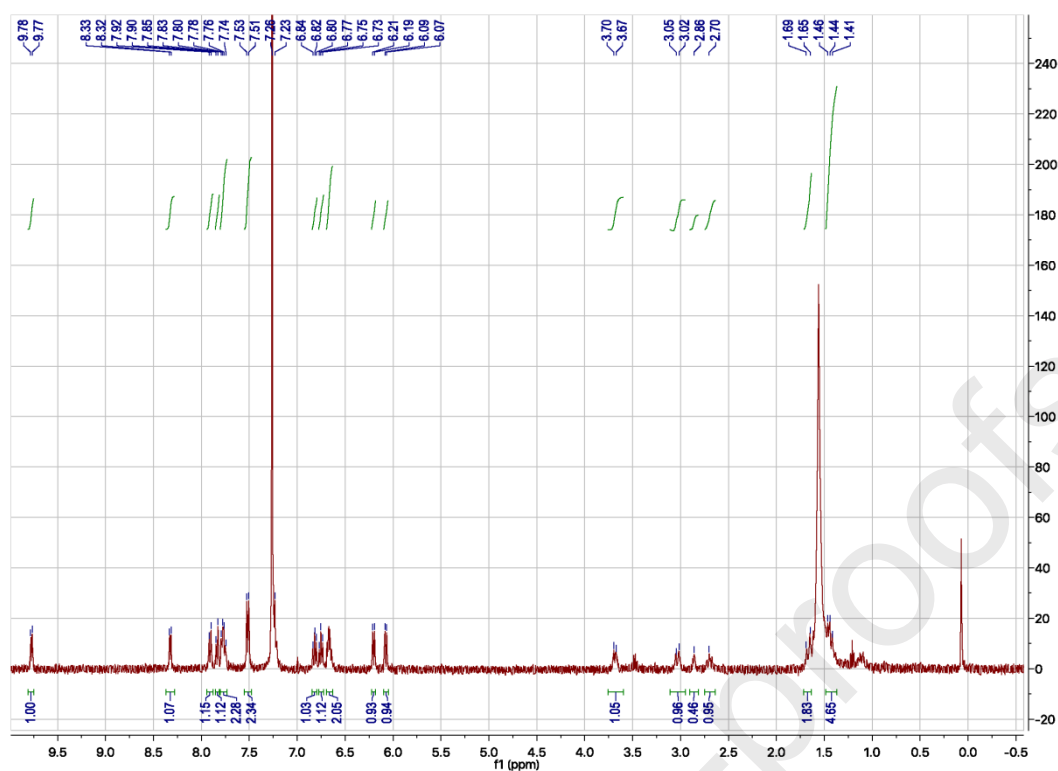
## 1.- NMR Characterization



**Figure S1.** <sup>1</sup>H NMR (300 MHz) in CDCl<sub>3</sub> of the product of the reaction of compound **2** (up), and the NMR of the same sample adding an excess of *t*-BuNH<sub>2</sub> (down). In the middle, for comparison, the spectrum of the complex [Ir(ppy)<sub>2</sub>Cl]<sub>2</sub>.

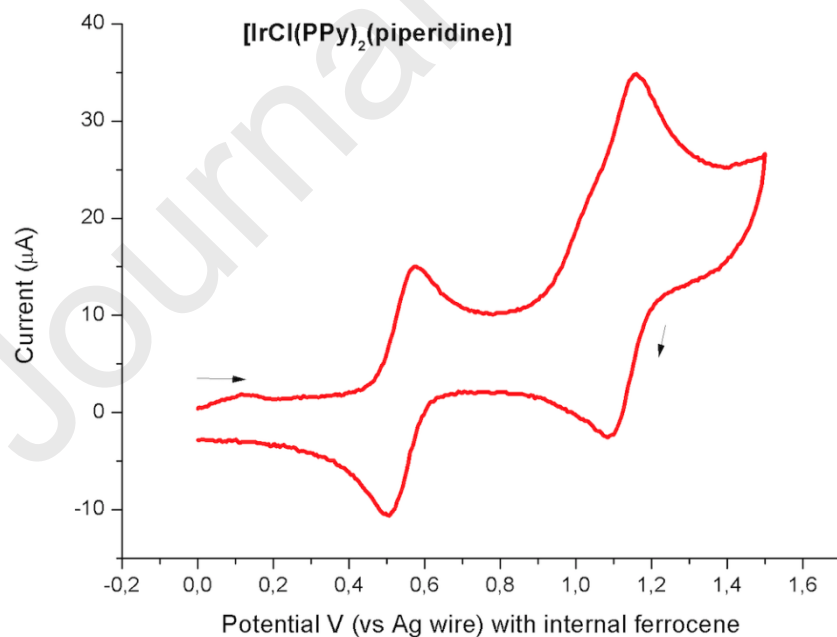


**Figure S2.** <sup>1</sup>H NMR (400 MHz) in CDCl<sub>3</sub> of the product of the reaction of compound **1**.

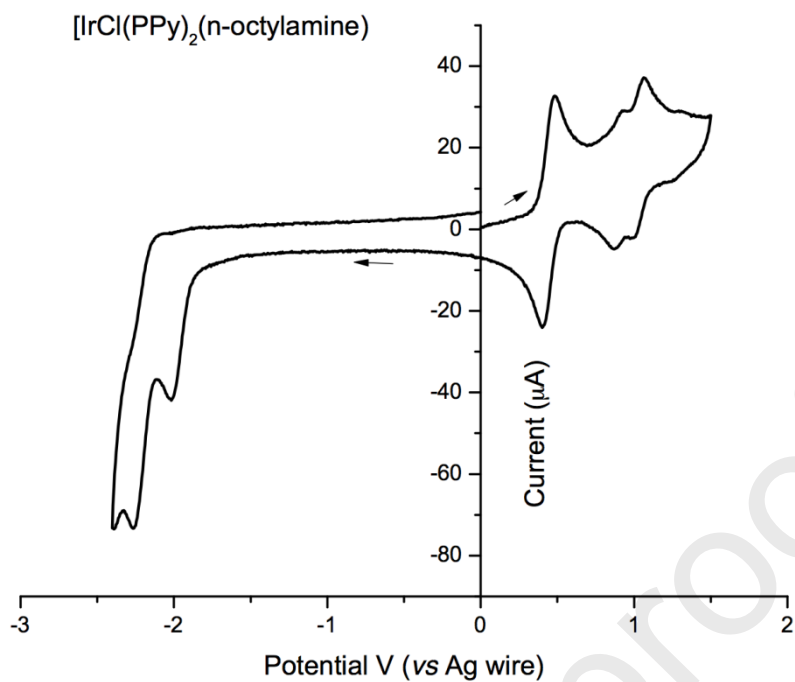


**Figure S3.**  $^1\text{H}$  NMR (400 MHz) in  $\text{CDCl}_3$  of the product of the reaction of compound 3.

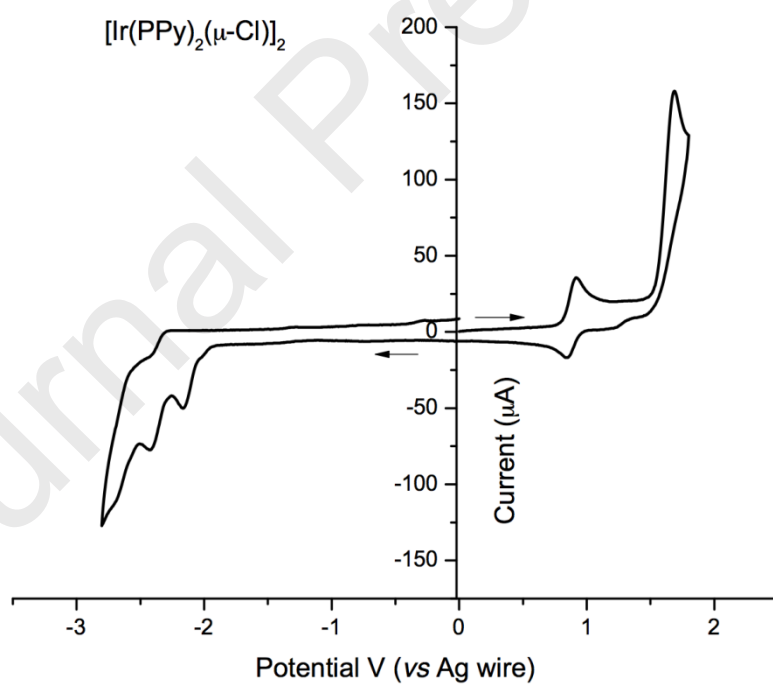
## 2.- Electrochemistry:



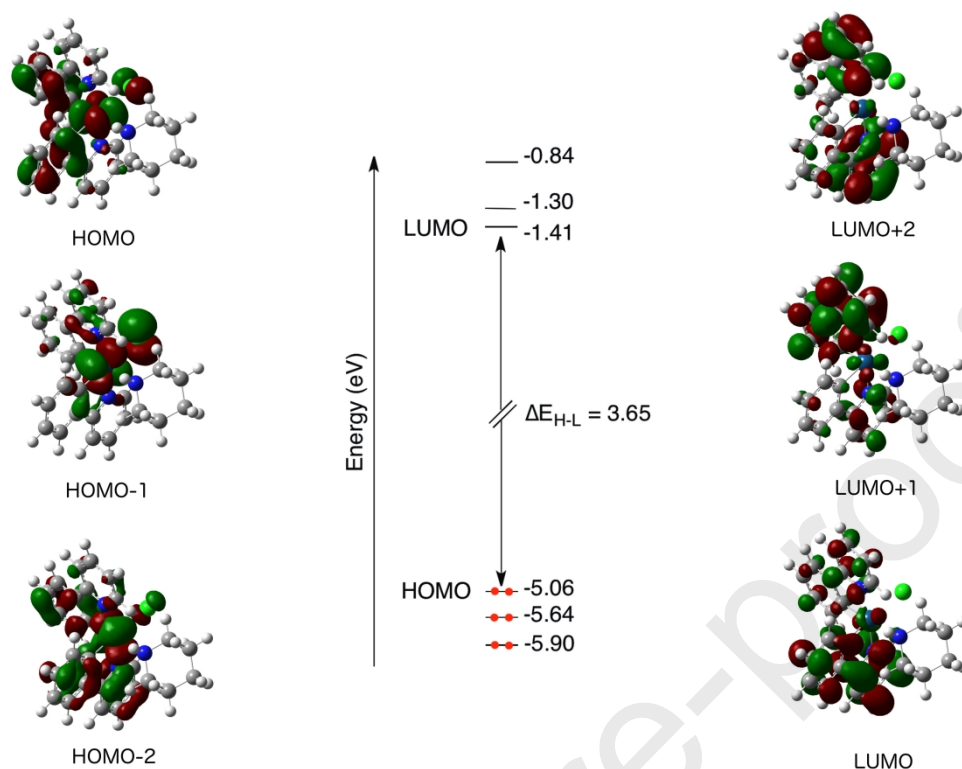
**Figure S4.** Anodic cyclic scan of  $10^{-3}\text{M}$   $[\text{IrCl}(\text{ppy})_2(\text{piperidine})](3)$  in acetonitrile with ferrocene added as internal calibrant.



**Figure S5.** Cyclic voltammograms of 1.1 mM  $[\text{IrCl}(\text{ppy})_2(\text{n-octylamine})](1)$  in acetonitrile with ferrocene added as internal calibrant.



**Figure S6.** Cyclic voltammograms of 0.9 mM  $[\text{Ir}_2(\text{ppy})_4(\mu\text{-Cl})_2]$  in acetonitrile with ferrocene added as internal calibrant.

**3.- Quantum Chemical Calculations.**

**Figure S7.** Schematic representation showing the frontier molecular orbitals ( $0.3 \text{ e}\cdot\text{au}^{-3}$ ) for compound **3** and their calculated energies (eV).

**Table S1.** Cartesian coordinates of **1** ( $S_0$ ).

Center Number	Atomic Number	Atomic Type	Coordinates (Angstroms)		
			X	Y	Z
1	77	0	1.04908	-0.254194	-0.04304
2	6	0	3.726536	-1.461759	-0.261853
3	6	0	2.442238	-2.651296	1.296996
4	6	0	4.794996	-2.346428	-0.051898
5	6	0	3.469124	-3.551423	1.542361
6	1	0	1.493109	-2.755863	1.806779
7	6	0	4.673534	-3.391427	0.853436
8	1	0	5.71722	-2.21029	-0.604708
9	1	0	3.319009	-4.356122	2.253925
10	1	0	5.501482	-4.075233	1.015694
11	6	0	2.512973	0.397977	-1.273847
12	6	0	2.479165	1.477136	-2.176514
13	6	0	3.728967	-0.336831	-1.198436
14	6	0	3.585063	1.811648	-2.961827
15	1	0	1.575107	2.071009	-2.276725
16	6	0	4.842245	0.003042	-1.987658

17	6	0	4.773429	1.077114	-2.869464
18	1	0	5.634005	1.339604	-3.478938
19	6	0	1.510385	1.124926	1.349178
20	6	0	0.742652	2.322462	1.28391
21	6	0	2.454182	1.023201	2.386834
22	6	0	0.916607	3.352651	2.223975
23	6	0	2.624086	2.049872	3.320313
24	1	0	3.067374	0.129744	2.473604
25	6	0	1.855887	3.217967	3.243077
26	1	0	1.990457	4.014633	3.969717
27	6	0	-1.105097	1.193545	-1.641111
28	6	0	-0.223232	2.386072	0.183693
29	6	0	-1.931102	2.251628	-1.996626
30	1	0	-1.079352	0.263718	-2.197153
31	6	0	-1.041144	3.479563	-0.132418
32	6	0	-1.898768	3.415671	-1.224215
33	1	0	-2.580268	2.158492	-2.86061
34	1	0	-0.994463	4.376495	0.474458
35	1	0	-2.529431	4.264028	-1.473562
36	7	0	2.556169	-1.62518	0.430347
37	7	0	-0.275523	1.251984	-0.57999
38	1	0	3.361859	1.940148	4.112469
39	1	0	5.764385	-0.567669	-1.918189
40	1	0	3.521687	2.651742	-3.650583
41	1	0	0.321768	4.260542	2.164401
42	6	0	-1.794807	-0.588761	1.716886
43	1	0	-2.089908	-0.885144	2.732259
44	1	0	-1.699255	0.500625	1.7124
45	7	0	-0.453805	-1.170158	1.413514
46	1	0	0.057765	-1.231151	2.293661
47	17	0	0.164428	-2.022181	-1.721322
48	1	0	-0.584987	-2.130058	1.089464
49	6	0	-2.867584	-1.046731	0.730883
50	1	0	-2.579995	-0.767331	-0.288926
51	1	0	-2.920312	-2.145397	0.750469
52	6	0	-4.247868	-0.466308	1.067503
53	1	0	-4.199403	0.632045	1.036313
54	1	0	-4.509818	-0.733286	2.102216
55	6	0	-5.357611	-0.953593	0.125852
56	1	0	-5.117272	-0.65597	-0.905478
57	1	0	-5.377174	-2.053537	0.130117
58	6	0	-6.748682	-0.423752	0.499836
59	1	0	-6.733625	0.676523	0.492522
60	1	0	-6.979827	-0.718943	1.534474
61	6	0	-7.865503	-0.92179	-0.42743
62	1	0	-7.646395	-0.613465	-1.460771

63	1	0	-7.868955	-2.022258	-0.431785
64	6	0	-9.260475	-0.416785	-0.034242
65	1	0	-9.261336	0.682888	-0.033094
66	1	0	-9.477631	-0.723782	0.99917
67	6	0	-10.37061	-0.925366	-0.95921
68	1	0	-11.354219	-0.552874	-0.647615
69	1	0	-10.205536	-0.601521	-1.994924
70	1	0	-10.415909	-2.022182	-0.959546

**Table S2.** Cartesian coordinates of **1** (T<sub>1</sub>).

Center Number	Atomic Number	Atomic Type	Coordinates (Angstroms)		
			X	Y	Z
1	77	0	1.211602	-0.125558	-0.289341
2	6	0	3.62549	-1.784487	0.041079
3	6	0	1.714559	-3.110399	0.334328
4	6	0	4.438782	-2.903366	0.267242
5	6	0	2.473219	-4.250608	0.561792
6	1	0	0.632956	-3.154049	0.347773
7	6	0	3.86484	-4.140419	0.53224
8	1	0	5.516795	-2.79963	0.231385
9	1	0	1.977663	-5.195365	0.756807
10	1	0	4.493311	-5.00794	0.709858
11	6	0	3.097058	0.549868	-0.476788
12	6	0	3.510463	1.856441	-0.790076
13	6	0	4.104392	-0.43433	-0.271749
14	6	0	4.864386	2.178705	-0.896333
15	1	0	2.76903	2.631173	-0.956883
16	6	0	5.464511	-0.104243	-0.378252
17	6	0	5.843935	1.199391	-0.690282
18	1	0	6.897549	1.451497	-0.773609
19	6	0	1.025238	0.440298	1.599117
20	6	0	0.436737	1.77857	1.754581
21	6	0	1.386752	-0.280508	2.749045
22	6	0	0.280991	2.303156	3.075444
23	6	0	1.199577	0.244975	4.028243
24	1	0	1.827108	-1.268615	2.642977
25	6	0	0.647753	1.548785	4.170634
26	1	0	0.513324	1.961324	5.168321
27	6	0	0.026996	2.246546	-1.814916
28	6	0	0.08176	2.447273	0.562493
29	6	0	-0.529251	3.506676	-1.955025
30	1	0	0.250268	1.62312	-2.674118
31	6	0	-0.490876	3.747896	0.447091
32	6	0	-0.795885	4.278003	-0.781737
33	1	0	-0.751764	3.88622	-2.94636

34	1	0	-0.68076	4.316193	1.35251
35	1	0	-1.230208	5.270109	-0.863364
36	7	0	2.265658	-1.906937	0.093715
37	7	0	0.329527	1.706134	-0.618907
38	1	0	1.478161	-0.325878	4.909278
39	1	0	6.231984	-0.856948	-0.222005
40	1	0	5.159849	3.196179	-1.141219
41	1	0	-0.131793	3.297363	3.221287
42	7	0	-0.878399	-1.088613	-0.172004
43	1	0	-0.924297	-1.618122	0.700454
44	17	0	1.053329	-0.920865	-2.726222
45	1	0	-0.86675	-1.774824	-0.929424
46	6	0	-2.114181	-0.272761	-0.285404
47	1	0	-2.086985	0.476732	0.510571
48	1	0	-2.071538	0.258801	-1.239926
49	6	0	-3.395128	-1.105527	-0.189488
50	1	0	-3.390551	-1.665172	0.757643
51	1	0	-3.404501	-1.852075	-0.996951
52	6	0	-4.662322	-0.242428	-0.266842
53	1	0	-4.629684	0.516561	0.528493
54	1	0	-4.668728	0.308952	-1.218247
55	6	0	-5.959738	-1.051964	-0.138128
56	1	0	-6.001346	-1.803726	-0.940206
57	1	0	-5.94259	-1.613389	0.8079
58	6	0	-7.224768	-0.184301	-0.187501
59	1	0	-7.171177	0.576567	0.60554
60	1	0	-7.249547	0.367461	-1.139023
61	6	0	-8.525222	-0.983833	-0.030963
62	1	0	-8.586116	-1.741065	-0.827131
63	1	0	-8.496671	-1.540233	0.91806
64	6	0	-9.78788	-0.11203	-0.065553
65	1	0	-9.723247	0.648464	0.725966
66	1	0	-9.821297	0.43902	-1.016431
67	6	0	-11.082187	-0.913568	0.104108
68	1	0	-11.964434	-0.262542	0.070874
69	1	0	-11.193147	-1.663191	-0.690131
70	1	0	-11.098281	-1.44527	1.064358

**Table S3.** Cartesian coordinates of **3** ( $S_0$ ).

Center Number	Atomic Number	Atomic Type	Coordinates (Angstroms)		
			X	Y	Z
1	77	0	-0.117342	0.180868	-0.186046
2	6	0	-3.047649	0.458729	-0.002188
3	6	0	-2.027859	2.357496	0.910415
4	6	0	-4.309285	1.004992	0.277135

5	6	0	-3.25009	2.942525	1.208952
6	1	0	-1.108301	2.877572	1.141802
7	6	0	-4.417216	2.247676	0.885775
8	1	0	-5.201722	0.449144	0.014337
9	1	0	-3.27601	3.918931	1.680444
10	1	0	-5.394187	2.669864	1.102005
11	6	0	-1.448553	-1.187848	-0.827891
12	6	0	-1.185536	-2.425986	-1.44142
13	6	0	-2.812508	-0.836749	-0.64059
14	6	0	-2.218906	-3.269471	-1.856965
15	1	0	-0.160688	-2.742279	-1.610132
16	6	0	-3.850578	-1.687636	-1.060028
17	6	0	-3.556926	-2.903968	-1.668201
18	1	0	-4.35991	-3.560516	-1.992309
19	6	0	0.113255	-0.792741	1.562245
20	6	0	1.179584	-1.736528	1.585453
21	6	0	-0.630036	-0.635784	2.745635
22	6	0	1.47972	-2.469425	2.746249
23	6	0	-0.328615	-1.366646	3.898885
24	1	0	-1.457158	0.068833	2.774849
25	6	0	0.727827	-2.285021	3.903981
26	1	0	0.960336	-2.852278	4.801163
27	6	0	2.120658	-1.031578	-1.860256
28	6	0	1.933968	-1.856984	0.333929
29	6	0	3.169458	-1.894531	-2.148507
30	1	0	1.723986	-0.334755	-2.589493
31	6	0	2.991639	-2.744554	0.092362
32	6	0	3.613252	-2.766062	-1.15061
33	1	0	3.6216	-1.878989	-3.13439
34	1	0	3.31564	-3.419876	0.876091
35	1	0	4.429965	-3.456359	-1.34061
36	7	0	-1.911221	1.148829	0.32556
37	7	0	1.51893	-1.006465	-0.654111
38	1	0	-0.920433	-1.219153	4.79993
39	1	0	-4.889497	-1.403735	-0.916727
40	1	0	-1.979682	-4.218411	-2.332633
41	1	0	2.301069	-3.181217	2.753261
42	6	0	2.457963	3.295809	-1.026825
43	6	0	1.356075	3.229346	0.030334
44	6	0	2.632015	1.557617	1.298131
45	6	0	3.758222	1.588266	0.265483
46	6	0	3.82893	2.949881	-0.435408
47	1	0	1.53138	4.009093	0.788644
48	1	0	0.385572	3.412149	-0.434049
49	1	0	2.210006	2.603834	-1.8389
50	1	0	2.459807	4.306831	-1.453753

51	1	0	2.861226	2.284121	2.093835
52	1	0	2.551262	0.574498	1.765269
53	1	0	4.700795	1.361335	0.779421
54	1	0	3.600617	0.801534	-0.480295
55	1	0	4.12616	3.721428	0.290335
56	1	0	4.595254	2.938965	-1.220506
57	7	0	1.297008	1.901442	0.717086
58	1	0	0.70086	2.031618	1.53359
59	17	0	-0.252852	1.385846	-2.470694

**Table S4.** Cartesian coordinates of **3** ( $T_1$ ).

Center Number	Atomic Number	Atomic Type	Coordinates (Angstroms)		
			X	Y	Z
1	77	0	0.192802	-0.072331	-0.3547
2	6	0	3.087991	-0.422342	0.129775
3	6	0	2.072882	-2.52533	-0.034804
4	6	0	4.333922	-1.035981	0.318164
5	6	0	3.281246	-3.18491	0.143717
6	1	0	1.157901	-3.082926	-0.177842
7	6	0	4.434868	-2.421219	0.32901
8	1	0	5.219149	-0.42494	0.448654
9	1	0	3.307051	-4.269123	0.136829
10	1	0	5.399253	-2.898773	0.474113
11	6	0	1.517333	1.429211	-0.1692
12	6	0	1.249145	2.805096	-0.257509
13	6	0	2.857877	1.023222	0.068103
14	6	0	2.269522	3.74673	-0.112738
15	1	0	0.237457	3.148858	-0.444346
16	6	0	3.878547	1.976054	0.218727
17	6	0	3.585523	3.334407	0.128202
18	1	0	4.378146	4.068664	0.242791
19	6	0	-0.362419	0.043541	1.538355
20	6	0	-1.514091	0.929274	1.765249
21	6	0	0.244325	-0.576882	2.645944
22	6	0	-1.972133	1.120439	3.104874
23	6	0	-0.234503	-0.387711	3.940554
24	1	0	1.104807	-1.222014	2.489367
25	6	0	-1.349076	0.472728	4.151566
26	1	0	-1.716172	0.625298	5.164208
27	6	0	-1.864491	1.693252	-1.758111
28	6	0	-2.066467	1.533271	0.614128
29	6	0	-2.927636	2.575795	-1.834515
30	1	0	-1.319056	1.381197	-2.642004
31	6	0	-3.160103	2.4453	0.564357
32	6	0	-3.596264	2.960084	-0.631544

33	1	0	-3.232835	2.962729	-2.800692
34	1	0	-3.644635	2.731149	1.492855
35	1	0	-4.429642	3.655717	-0.663427
36	7	0	1.964826	-1.184467	-0.031885
37	7	0	-1.429386	1.16463	-0.597003
38	1	0	0.235312	-0.883716	4.784941
39	1	0	4.902791	1.666262	0.405291
40	1	0	2.038691	4.806854	-0.185894
41	1	0	-2.8152	1.77502	3.306389
42	6	0	-3.637702	-1.442977	-1.079352
43	6	0	-2.34831	-1.835213	-1.800143
44	6	0	-1.522929	-2.988258	0.206969
45	6	0	-2.790445	-2.609227	0.972277
46	6	0	-3.98527	-2.448627	0.025028
47	1	0	-2.510037	-2.788132	-2.32847
48	1	0	-2.062064	-1.08964	-2.544116
49	1	0	-3.528848	-0.444895	-0.642919
50	1	0	-4.442451	-1.38496	-1.822871
51	1	0	-1.658076	-3.981367	-0.249422
52	1	0	-0.674263	-3.047058	0.89291
53	1	0	-2.984452	-3.386211	1.722126
54	1	0	-2.620604	-1.672658	1.515526
55	1	0	-4.231656	-3.421842	-0.424566
56	1	0	-4.872573	-2.119573	0.579603
57	7	0	-1.192722	-2.006291	-0.868063
58	1	0	-0.457813	-2.42194	-1.440732
59	17	0	0.711001	-0.34047	-2.860014

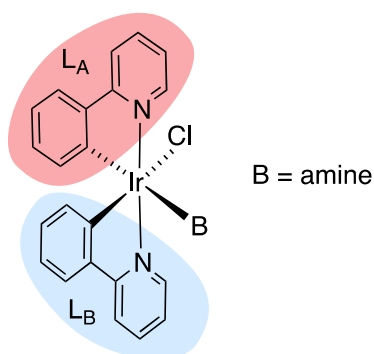


Chart S1

**Table S5.** B3LYP/(6-31G\*\*+LANL2DZ) composition (in %) calculated for the HOMO-2 to the LUMO+2 orbitals of complexes **1** and **3** in the singlet ground state ( $S_0$ ).  $L_A$  and  $L_B$  denote the cyclometalating ligands (see Chart S1).

Complex		HOMO-2	HOMO-1	HOMO	LUMO	LUMO+1	LUMO+2
<b>1</b>	Ir	65,55	0,00	53,08	4,27	5,61	3,53
	$L_A$	11,80	0,15	20,15	20,30	71,28	42,19
	$L_B$	19,28	0,14	18,37	71,89	20,73	51,27
	Amine	1,59	0,01	1,00	3,03	0,74	2,79
	Cl	1,78	0,00	7,39	0,51	1,64	0,22
<b>3</b>	Ir	53,35	58,64	54,06	4,71	5,46	4,66
	$L_A$	19,64	8,32	17,99	18,90	73,09	42,57
	$L_B$	21,90	8,67	18,68	72,55	19,31	49,23
	Amine	1,24	0,34	1,14	3,26	0,69	3,33
	Cl	3,87	24,03	8,13	0,58	1,44	0,22

**Table S6.** Unpaired-electron spin-density distributions computed for the fully relaxed  $T_1$  or  $T_2$  states of complexes **1** and **3**.

Complex	Ir	Ir	$L_A$	$L_B$	Cl	amine
<b>1</b>	$T_1$	0.440343	0.070325	1.452134	0.027143	0.010055
<b>3</b>	$T_1$	0.451053	0.056689	1.453177	0.023296	0.01579

## 4.- ESI\_HRMS:

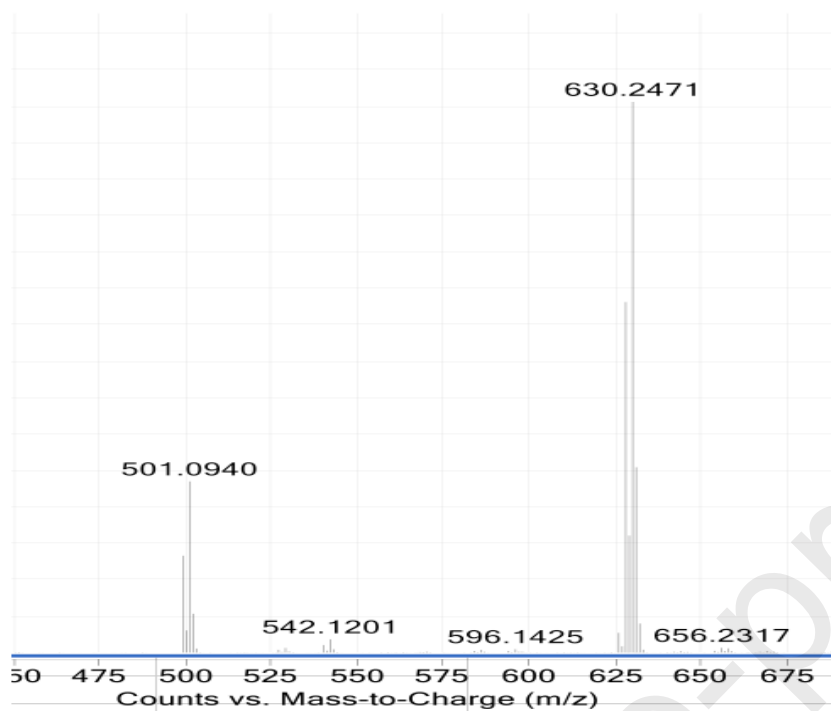


**Figure S8.** ESI-HRMS of compound **1**. ESI-HRMS Calculated ( $[M-Cl]^+$ )  $m/z$  630.2460, found ( $[M-Cl]^+$ )  $m/z$  630.2471. ESI-HRMS Calculated ( $[Ir(ppy)_2]^+$ )  $m/z$  501.0943, found ( $[Ir(ppy)_2]^+$ )  $m/z$  501.0940.

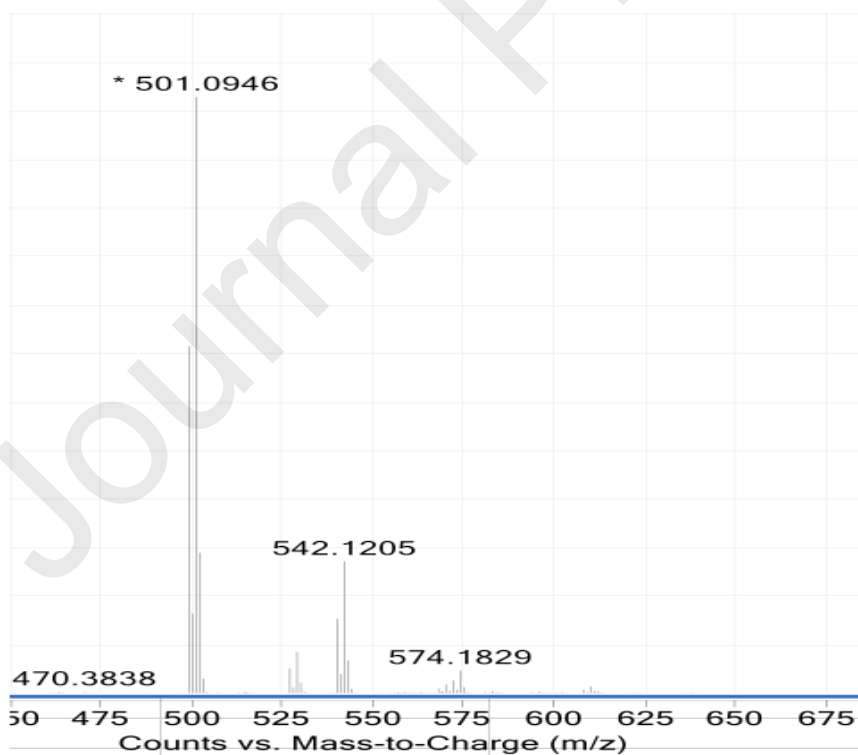


**Figure S9.** ESI-HRMS of compound **2**. ESI-HRMS Calculated ( $[M-Cl]^+$ )  $m/z$  574.1834, found ( $[M-Cl]^+$ )  $m/z$  574.1829. ESI-HRMS Calculated ( $[Ir(ppy)_2]^+$ )  $m/z$  501.0943, found ( $[Ir(ppy)_2]^+$ )  $m/z$  501.0940.

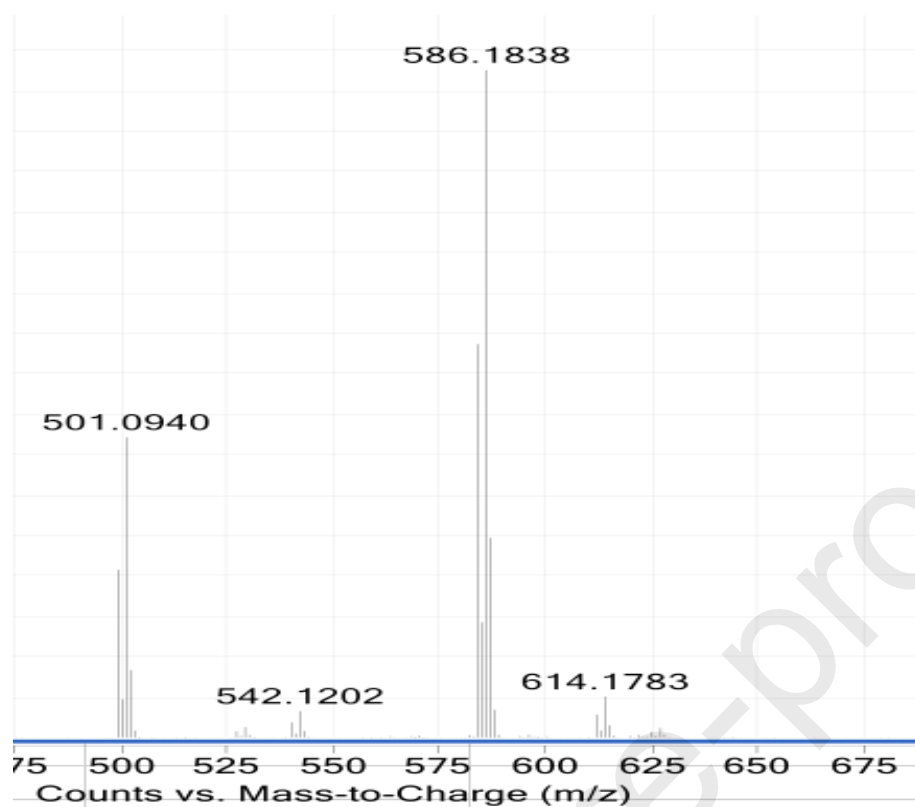
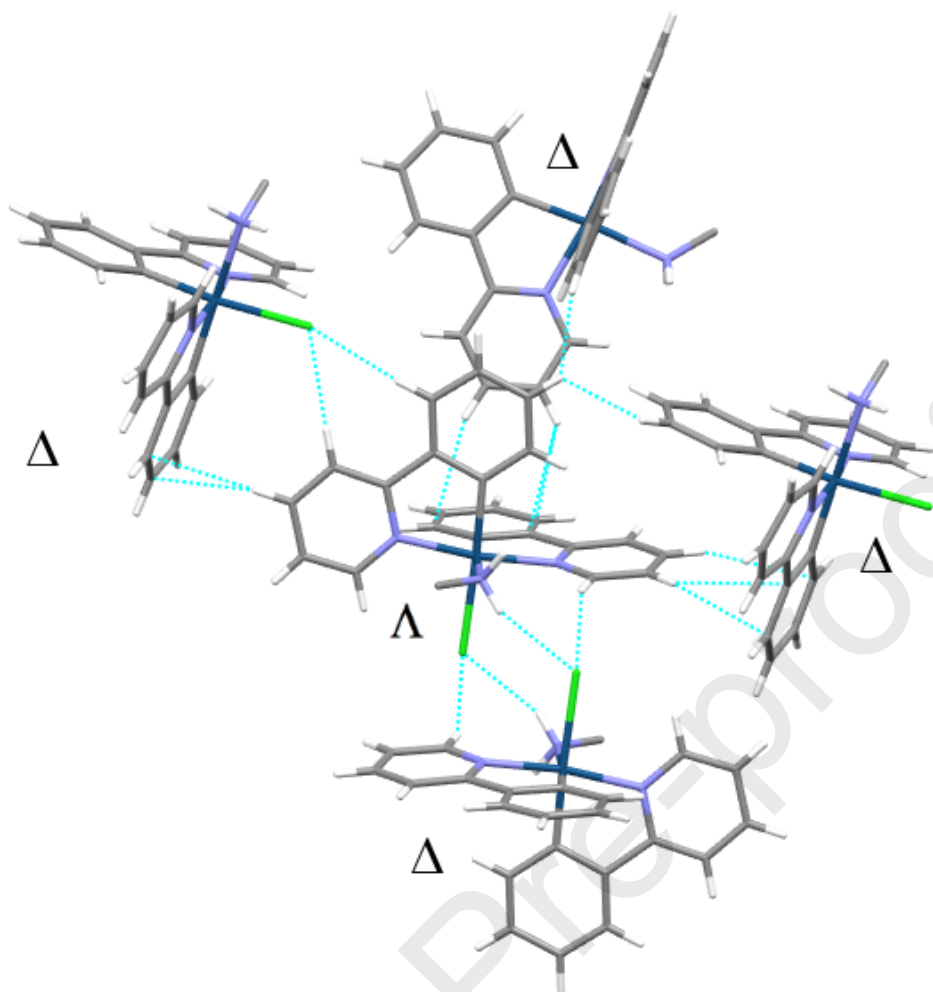


**Figure S10.** ESI-HRMS of compound **3**. ESI-HRMS Calculated ( $[\text{M}-\text{Cl}]^+$ )  $m/z$  586.1834, found ( $[\text{M}-\text{Cl}]^+$ )  $m/z$  586.1838. ESI-HRMS Calculated ( $[\text{Ir}(\text{ppy})_2]^+$ )  $m/z$  501.0943, found ( $[\text{Ir}(\text{ppy})_2]^+$ )  $m/z$  501.0940.

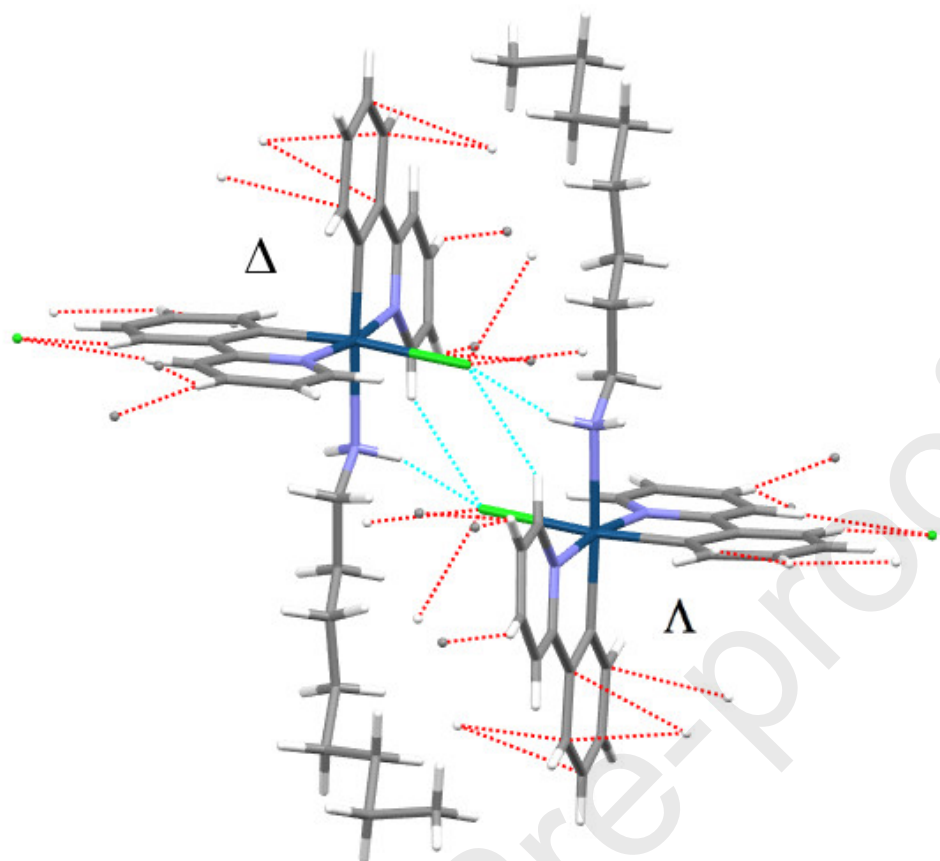
## 5.- Structural Characterization

Table S7. Crystal data and structure refinement for complex 1.

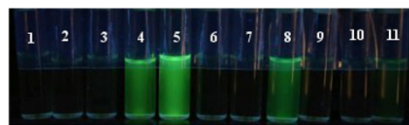
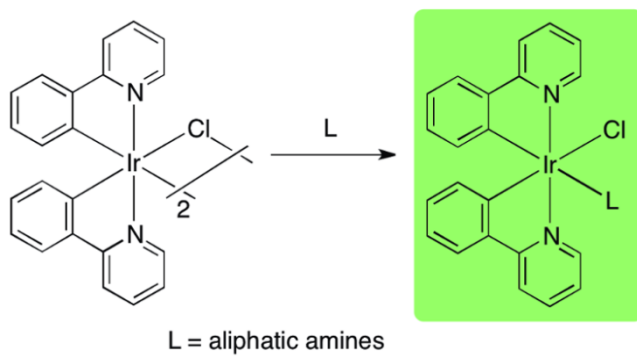
Empirical formula	$C_{30}H_{37}ClIrN_3$
Formula weight	665.26
Temperature [K]	100(2)
Wavelength [ $\text{\AA}$ ]	0.71073
Crystal system	Trigonal
Space group	R-3
$a$ [ $\text{\AA}$ ]	22.6266(3)
$B$ [ $\text{\AA}$ ]	22.6266(3)
$C$ [ $\text{\AA}$ ]	28.4199(5)
$\alpha$ [ $^\circ$ ]	90.00
$\beta$ [ $^\circ$ ]	90.00
$\gamma$ [ $^\circ$ ]	120.00
Volume [ $\text{\AA}^3$ ]	12600.6(4)
$Z$	18
Density (calculated) [ $\text{Mg/m}^3$ ]	1.578
Absorption coefficient [ $\text{mm}^{-1}$ ]	4.886
$F(000)$	5940
Crystal size [ $\text{mm}^3$ ]	0.1 x 0.1 x 0.05
$\theta$ range for data collection [ $^\circ$ ]	2.53-27.51
Index ranges	$-29 \leq h \leq 29$ $-29 \leq k \leq 27$ $-36 \leq l \leq 36$
Reflections collected	39633
Independent reflections	6416 [ $R_{\text{int}} = 0.0285$ , $R_{\text{sigma}} = 0.0182$ ]
Data/restraints/parameters	6416/0/275
Min. and max. transmission	0.648 and 0.7922
Goodness-of-fit on $F^2$	1.033
$R$ indices [ $I > 2\sigma(I)$ ]	$R_1 = 0.0315$ , $wR_2 = 0.0807$
$R$ indices (all data)	$R_1 = 0.0355$ , $wR_2 = 0.0844$
Largest diff. peak and hole [ $e\text{\AA}^{-3}$ ]	3.00 and $-1.47$



**Figure S11.** Weak interactions between  $\Lambda$ -1 and the surrounding neighbors (all of them with the  $\Delta$  absolute configuration).



**Figure S12.** Weak interactions between  $\Delta$  and  $\Delta$  showing as the n-octyl chains do not interact with neighbor molecules.



L = Biogenic amines

Journal Pre-proofs

## HIGHLIGHTS

- Straightforward synthesis of Ir(III) complexes with aliphatic amines is reported.
- These complexes display strong luminescence around 510 nm.
- The reaction of formation of these complexes is useful to detect biogenic amines.